University Library

MINERVA ACCESS

A gateway to Melbourne's research publications

Minerva Access is the Institutional Repository of The University of Melbourne

Author/s:
Fabian, SG;Gallagher, SJ;De Vleeschouwer, D

Title:
British–Irish Ice Sheet and polar front history of the Goban Spur, offshore southwest Ireland over the last 250 000 years

Date:
2023-10-01

Citation:
Fabian, S. G., Gallagher, S. J. & De Vleeschouwer, D. (2023). British–Irish Ice Sheet and polar front history of the Goban Spur, offshore southwest Ireland over the last 250 000 years. Boreas, 52 (4), pp.476-497. https://doi.org/10.1111/bor.12631.

Persistent Link:
https://hdl.handle.net/11343/336985

License:
CC BY

Check for updates

BOREAS An international journal of Quaternary research

British–Irish Ice Sheet and polar front history of the Goban Spur, offshore southwest Ireland over the last 250 000 years

STANISLAUS G. FABIAN, STEPHEN J. GALLAGHER AND DAVID DE VLEESCHOUWER

BOREAS

Fabian, S. G., Gallagher, S. J. & De Vleeschouwer, D.: British–Irish Ice Sheet and polar front history of the Goban Spur, offshore southwest Ireland over the last 250 000 years. *Boreas*. https://doi.org/10.1111/bor.12631. ISSN 0300-9483.

Deep Sea Drilling Program (DSDP) Site 548 was cored in 1984 at a water depth of 1256 m on the Goban Spur, offshore southwest Ireland. Coring retrieved a ~100-m-thick Pleistocene contourite sequence. This study uses planktonic foraminiferal assemblage and benthic foraminiferal oxygen isotope analyses to establish an age model for the upper 40 m of this core. This site's multidisciplinary analyses of planktonic foraminiferal assemblages, lithic grains, facies and calcium carbonate concentration reveal a 250 000-year record of the North Atlantic polar front variability and British–Irish Ice Sheet (BIIS) history. The sequence is characterized by alternations of ice rafted debris (IRD) laden pelagic mud facies with calcium carbonate-rich silty sand contourite facies that track glacial/interglacial cycles. The polar front migrated southward across the area several times during glacial maxima and stadial periods, while warmer Mediterranean Outflow Water (MOW) flowed northward across the region during interglacial and interstadial periods depositing contourites. Lithic analyses reveal a complex history of IRD deposition associated with iceberg calving from the Laurentide Ice Sheet and northwest European ice sheets, mainly the BIIS. Comparison between the Goban Spur (DSDP Site 548) and the Celtic Margin (MD03-2692) and central North Atlantic Integrated Ocean Drilling Program (IODP) Site U1308 suggests differences between the 'non-Laurentide Ice Sheet' Heinrich Events (HE) 6 and 3 at the Goban Spur, with IRD from the BIIS being prominent during HE 6 and IRD from other European ice sheets north of the BIIS likely being more dominant during HE 3. The nature of lithics in IRD-rich horizons during Terminations 3, 3A, 2 and 1 suggests significant iceberg calving episodes preceding BIIS retreat during the onset of interstadial intervals.

Stanislaus G. Fabian (stglenn49@gmail.com) and Stephen J. Gallagher, School of Geography, Earth and Atmospheric Sciences, McCoy Building, Corner Swanston & Elgin Streets, The University of Melbourne, Parkville, VIC 3010, Australia; David De Vleeschouwer, Institute of Geology and Paleontology, University of Münster, Corrensstr 24, 48149 Münster, Germany; *received 13th March 2023, accepted 29th June 2023.*

Rapid late Cenozoic climatic variations markedly affected global oceanography and ice-sheet behaviour in the North Atlantic Ocean and are well recorded in marine sedimentary strata (Ruddiman *et al*. 1989) and ice-cores (Grootes *et al*. 1993). In particular, the area around Greenland and northeastern Canada hosts the North Atlantic polar front (Fig. 1), a physical oceanographic feature separating two surface water-masses: cold, low-salinity modified Polar Water and warmer high-salinity Atlantic Water (Eynaud *et al*. 2007; Holliday *et al*. 2008). In the past, the polar front migrated southwards as far as the Iberian Margin (Eynaud *et al*. 2009; Fig. 1). The dynamics of the polar front in the northeast Atlantic Ocean during periods of rapid climatic variability have been the subject of several studies (Eynaud *et al*. 2009; Bashirova *et al*. 2014; Marchal *et al*. 2016). A few studies have documented the polar front history on the Celtic Margin (Scourse *et al*. 2000; Mojtahid *et al*. 2005). However, these studies do not document its history beyond the last glacial cycle.

One result of the climate oscillations in the North Atlantic is the waxing, waning and eventual demise of the British–Irish Ice Sheet (BIIS). The BIIS is a historical ice sheet that periodically covered parts of Britain and Ireland since the Early Pleistocene (~2.5 Ma; Peters *et al*. 2015; Scourse *et al*. 2021; Clark *et al*. 2022; Gibbard *et al*. 2022; Fig. 2). The Quaternary evolution and estimates of the maximum extent of the BIIS have been the subject of several studies (Knutz *et al*. 2007; Scourse *et al*. 2009, 2021; Thierens *et al*. 2012; Peters *et al*. 2015, 2016; Clark *et al*. 2022). Despite this, the history of the BIIS is not as well known prior to the last glacial cycle (Gibbard *et al*. 2022). After the Middle Pleistocene, at least three stable ice-sheet phases during different glacial periods covered Britain and Ireland, the Anglian Ice Sheet (MIS 12) (Toucanne *et al*. 2009), Wolstonian Ice Sheet (MIS 10–6) and the Devensian Ice Sheet (MIS 5d–MIS 2) (Lee *et al*. 2011) (Fig. 2, Table 1).

The Wolstonian BIIS (Fig. 2) spanned multiple glacial cycles from MIS 10–6 (Gibbard *et al*. 2022), and during its maximum, it expanded eastwards in the North Sea and combined with Drenthe glaciation in the Netherlands (Gibbard *et al*. 2009, 2022; Moreau *et al*. 2012). The detailed history of the Wolstonian BIIS inception, demise and the history of its older phases are not well known, including records from MIS 7d, an anomalous stadial event (Toucanne *et al*. 2009; Hughes *et al*. 2020) within the interglacial MIS 7. The last BIIS phase, known as the Devensian (MIS 5d–MIS 2; Fig. 2), has been studied extensively (Eynaud *et al*. 2007; Clark *et al*. 2012; Peters *et al*. 2016; Bradwell *et al*. 2021; Scourse *et al*. 2021). Its evolution between 30 000–15 000 years ago is

DOI 10.1111/bor.12631
© 2023 The Authors. *Boreas* published by John Wiley & Sons Ltd on behalf of The Boreas Collegium. This is an open access article under the terms of the Creative Commons Attribution License, which permits use, distribution and reproduction in any medium, provided the original work is properly cited.

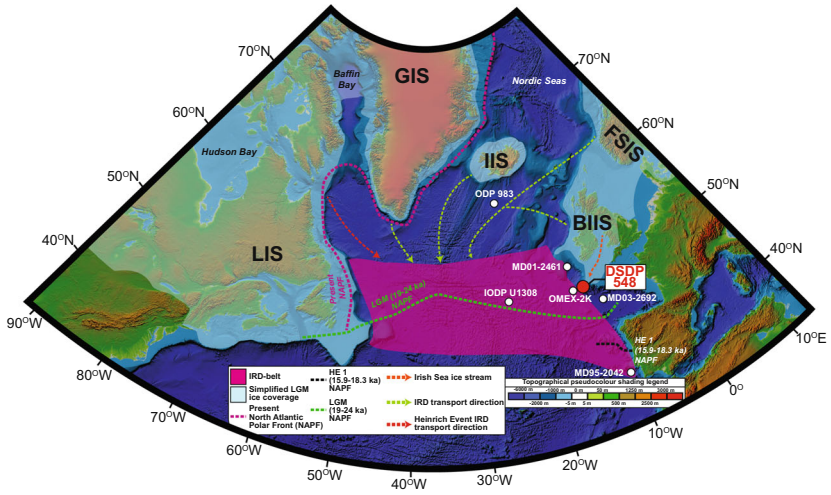

Fig. 1. Schematic diagram showing the location of Ruddiman's IRD belt (Andrews 2000), IRD transport direction (Peck *et al.* 2006), present and past polar front (PF) positions, Last Glacial Maximum (LGM) ice-sheet extent, and sites: Deep Sea Drilling Program (DSDP) Site 548 (De Graciansky *et al.* 1985), Integrated Ocean Drilling Program (IODP) Site U1308 (Hodell *et al.* 2008), Ocean Drilling Program (ODP) 983 (Barker *et al.* 2019), MD03-2692 (Toucanne *et al.* 2009), MD95-2042 (Shackleton *et al.* 2003), OMEX-2K (Haapaniemi *et al.* 2010) and MD01-2461 (Peck *et al.* 2007; Scourse *et al.* 2009). LIS = Laurentide Ice Sheet; GIS = Greenland Ice Sheet; IIS = Icelandic Ice Sheet; FSIS = Fennoscandian Ice Sheet; BIIS = British–Irish Ice Sheet. LIS and GIS LGM ice limits are modified after Dalton *et al.* (2020) with findings from Couette *et al.* (2022) for the Baffin Bay region. BIIS LGM ice limits are from Clark *et al.* (2022). IIS and FSIS LGM ice limits are modified after Hughes *et al.* (2022). Present-day and HE 1 (15.9–18.3 ka) North Atlantic polar front position is adapted from Eynaud *et al.* (2009), LGM polar front position is modified from Barker *et al.* (2015). Irish Sea Ice Stream (ISIS) flow direction is adapted from Scourse *et al.* (2021).

chronicled in detail by the BRITICE-CHRONO project (Clark *et al.* 2022), but its pre-LGM history is not as well known due to the sparseness of associated terrestrial glacial deposits (Gibbard *et al.* 2022). Thus, looking at proximal marine sedimentary records is necessary to fill in the gaps of the BIIS chronicle, particularly those older than the last glaciation cycle.

One result of the interaction between abrupt climatic oscillations and ice-sheet bodies in the North Atlantic is the periodic deposition of coarse-grained lithics from calving ice sheets known as ice rafted debris (IRD), such as those deposited within an area known as Ruddiman's IRD Belt (Ruddiman *et al.* 1989) during Heinrich Events (HE) (Heinrich 1988). Mud-rich marine sediments

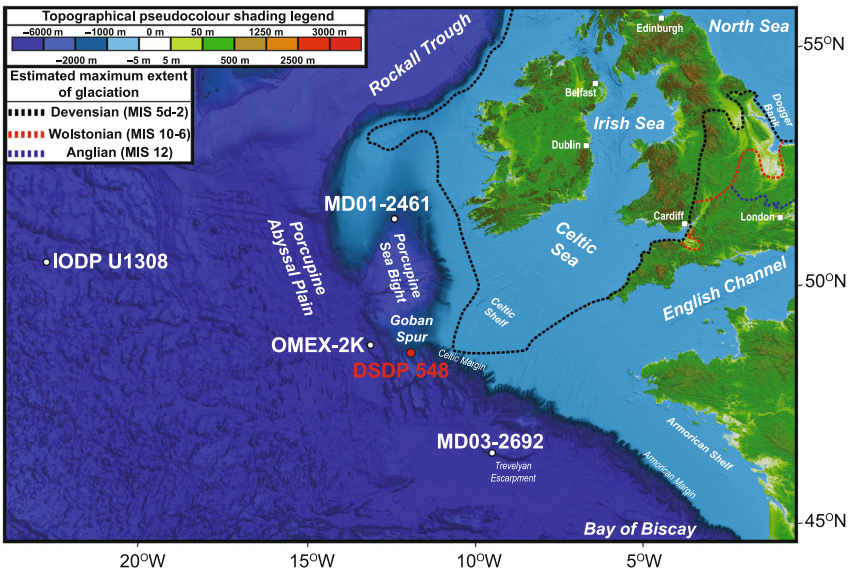

Fig. 2. The ice limits of the three phases of the BIIS glaciation and the location of other sites: DSDP Site 548 (De Graciansky *et al.* 1985), IODP Site U1308 (Hodell *et al.* 2008), MD03-2692 (Toucanne *et al.* 2009), OMEX-2K (Haapaniemi *et al.* 2010) and MD01-2461 (Peck *et al.* 2007; Scourse *et al.* 2009). The Devensian Ice Sheet limit is adapted from Clark *et al.* (2022). The Wolstonian and Anglian limits are adapted from Hughes *et al.* (2022).

15023885, 0, Downloaded from https://onlinelibrary.wiley.com/doi/10.1111/bor.12631 by National Health And Medical Research Council, Wiley Online Library on [10/08/2023]. See the Terms and Conditions (https://onlinelibrary.wiley.com/terms-and-conditions) on Wiley Online Library for rules of use; OA articles are governed by the applicable Creative Commons License

Table 1. Summary of Marine Isotope Stage names, general climatic conditions, and timing of the BIIS over the last 300 ka.

BIIS phase	Marine Isotope Stage		British stage name	General climatic condition	Start date (ka)		Reference
Absent	1		Holocene	Strong interglacial	11.7		Gibbard & Cohen (2008)
Devensian ice sheet	2		Devensian / Dimlington	Strong glacial	29		Delaney (2003); Hamblin *et al.* (2005); Railsback *et al.* (2015)
	3		Devensian (Middle)	Intermediate	57		
	4			Moderate glacial	71		
	5	a-d	Devensian (Early)	a & c: Moderate interglacial; b & d: Moderate glacial	130	119	
Absent		e	Ipswichian	Strong interglacial		124	Shackleton *et al.* (2003); Railsback *et al.* (2015)
Wolstonian ice sheet	6		Wolstonian	Strong glacial	191		Shotton (1983)
	7		Aveley	Moderate interglacial	243		Gibbard & Cohen (2008); Railsback *et al.* (2015)
	8		Wolstonian	Moderate glacial	300		Shotton (1983)

saturated with IRD from the Laurentide Ice Sheet (LIS; Fig. 1; Andrews & Voelker 2018) and *Neogloboquadrina pachyderma* dominant planktonic foraminifera assemblages associated with low foraminiferal productivity characterize HE (Heinrich 1988) in the North Atlantic (McCabe *et al.* 1998; Hodell *et al.* 2008; Stein *et al.* 2009; Ovsepyan & Murdmaa 2017). IRD records proximal to the past location of an ice sheet archive episodes of iceberg calving as demonstrated by Van Rooij *et al.* (2006), Peck *et al.* (2007) and Thierens *et al.* (2012), who interpreted BIIS iceberg calving since the Early Pleistocene using IRD records from the Porcupine Sea Bight.

An IRD record from MD01-2461 (Porcupine Sea Bight; Fig. 1) indicates, despite its proximity to the BIIS, multiple IRD sources other than the BIIS, including the LIS, Icelandic Ice Sheet and the Fennoscandian Ice Sheet (Peck *et al.* 2006). Haapaniemi *et al.* (2010) found minor yet distinct (<4% total IRD observed) peaks of LIS-sourced IRD in sediments coeval to HE 2 and 1, within predominantly BIIS and Irish Sea Ice Stream sourced IRD from OMEX-2K (down-slope, east Goban Spur) (Figs 1, 2). DSDP 548, another core from the Goban Spur (Fig. 1), is south of MD01-2461 and east of OMEX-2K; therefore, it is further from the LIS source, suggesting less IRD from the LIS. In addition, DSDP 548 is very close (~100 km east) to the maximum extent of the BIIS (Clark *et al.* 2022; Fig. 2) and directly downstream from the Irish Sea Ice Stream (Scourse *et al.* 2021; Fig. 1), making it an ideal archive for documenting IRD deposition from the BIIS with minimal influence of LIS sourced IRD.

DSDP Site 548's mud and marl sequences were suggested to be related to glacial–interglacial cycles but lacked age data for Marine Isotope Stages assignment (De Graciansky *et al.* 1985). Seismic profile interpretation at Site 548 identified Mediterranean Outflow Water (MOW) associated contourite sequences (Delivet *et al.* 2016). The strengthening of the MOW during interglacial periods (Kaboth *et al.* 2017) is associated with coarse-grained contourite sedimentation along its flow path (Van Rooij *et al.* 2010). Thus, the alternation of IRD-laden sediments with coarser contouritic sequences differentiates glacial–interglacial sediments of DSDP Core 548, warranting a more detailed age model to extract a detailed palaeoclimatic and palaeoceanographic history, including iceberg calving from the BIIS. This study thus has several aims. Firstly, to establish an age model for the upper 40 m of DSDP Site 548 based on benthic foraminiferal stable isotope correlation. Secondly, to identify the facies and their association with glacial–interglacial cycles. Thirdly, to examine the distribution of IRD lithics and their connection to Heinrich Events and BIIS iceberg calving periods. Lastly, to interpret the history of the BIIS and the polar front in the Goban Spur region for the past 250 000 years.

Setting

The Goban Spur (Williamson *et al.* 2011; Fig. 3A) is a topographic high seabed feature on the Celtic Margin 200 km offshore southwest Ireland, between 900 and 1600 m water depth (Colin *et al.* 1992). To the north, a gentle northwardly dipping slope connects it with the Porcupine Sea Bight, while two meandering submarine canyons erode its terraced western slope (Delivet *et al.* 2016). The eastern North Atlantic Ocean's continental margin between 26°N and 56°N is a 'glacially influenced margin' (Weaver *et al.* 2000) where underwater channels and canyons dominate the down-slope sedimentation

15023885, 0, Downloaded from https://onlinelibrary.wiley.com/doi/10.1111/bor.12631 by National Health And Medical Research Council, Wiley Online Library on [10/08/2023]. See the Terms and Conditions (https://onlinelibrary.wiley.com/terms-and-conditions) on Wiley Online Library for rules of use; OA articles are governed by the applicable Creative Commons License

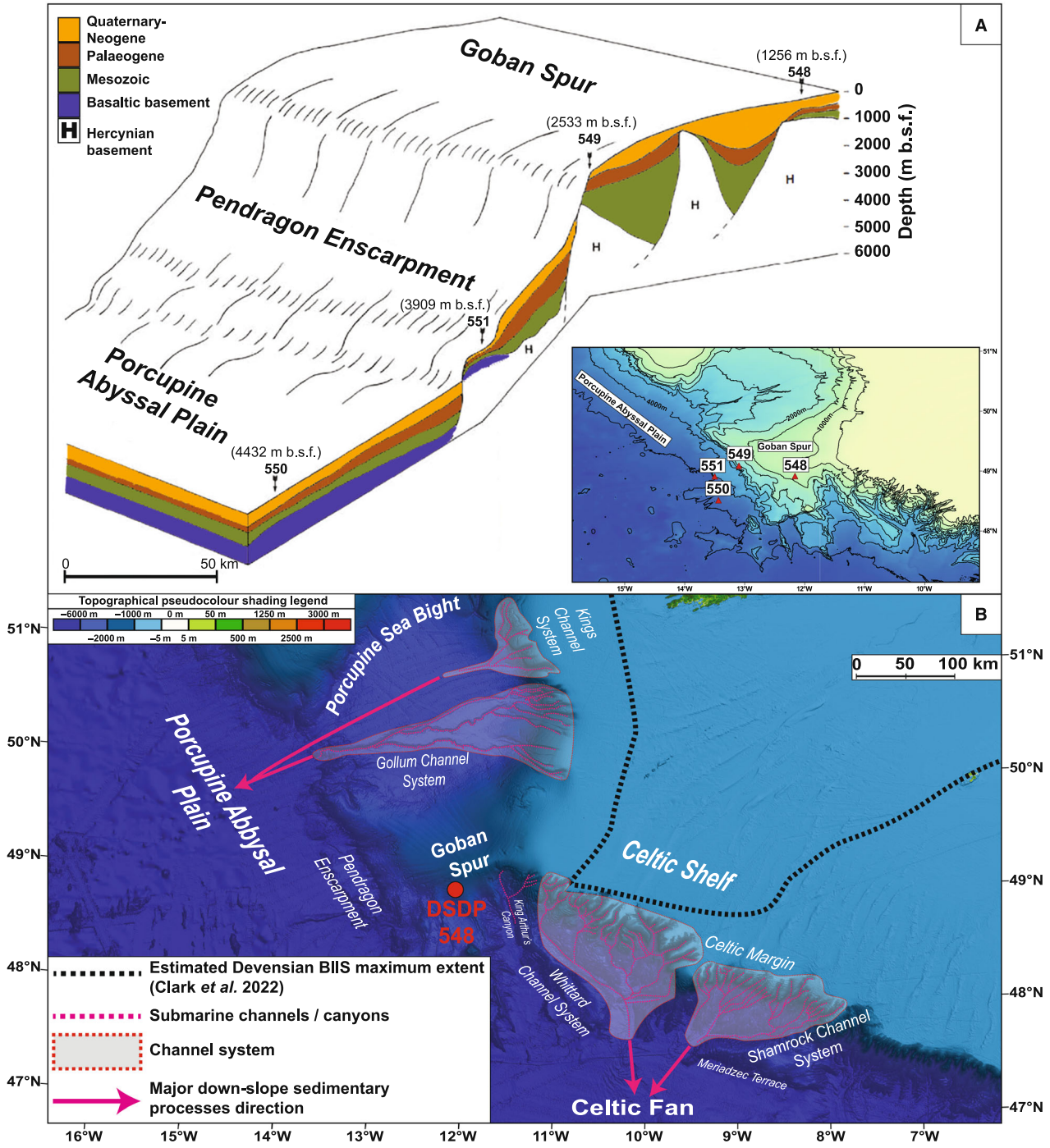

Fig. 3. A. Sea floor profile of the Goban Spur and inset map indicating the location of the coring site during DSDP Leg 80, including Site 548 (this study), modified after Snyder & Waters (1985). m b.s.f. = metres below the sea floor. B. Submarine canyons and channel systems around the Goban Spur adapted from Kenyon *et al.* (1978), Weaver *et al.* (2000) and Verweirder *et al.* (2021). BIIS limit is from Clark *et al.* (2022). DSDP Site 548 location is adapted from De Graciansky *et al.* (1985).

processes, particularly during glacial periods. The Goban Spur lacks submarine channel systems (Fig. 3B) and thus represents a low-energy environment protected from active down-slope processes and sedimentation (Loubere 1987), making it ideal for recording IRD deposition during the glacial period.

At present, several water-masses influence DSDP Site 548: the North Atlantic Current (Vigilante *et al.* 2017), Eastern North Atlantic Central Water, MOW and the Labrador Sea Water (Fig. 4A, B). The Eastern North Atlantic Central Water is a relatively saline (~35.5) and warm (10.5–11 °C) north-flowing current at ~500 m

15023885, 0, Downloaded from https://onlinelibrary.wiley.com/doi/10.1111/bor.12631 by National Health And Medical Research Council, Wiley Online Library on [10/08/2023]. See the Terms and Conditions (https://onlinelibrary.wiley.com/terms-and-conditions) on Wiley Online Library for rules of use; OA articles are governed by the applicable Creative Commons License

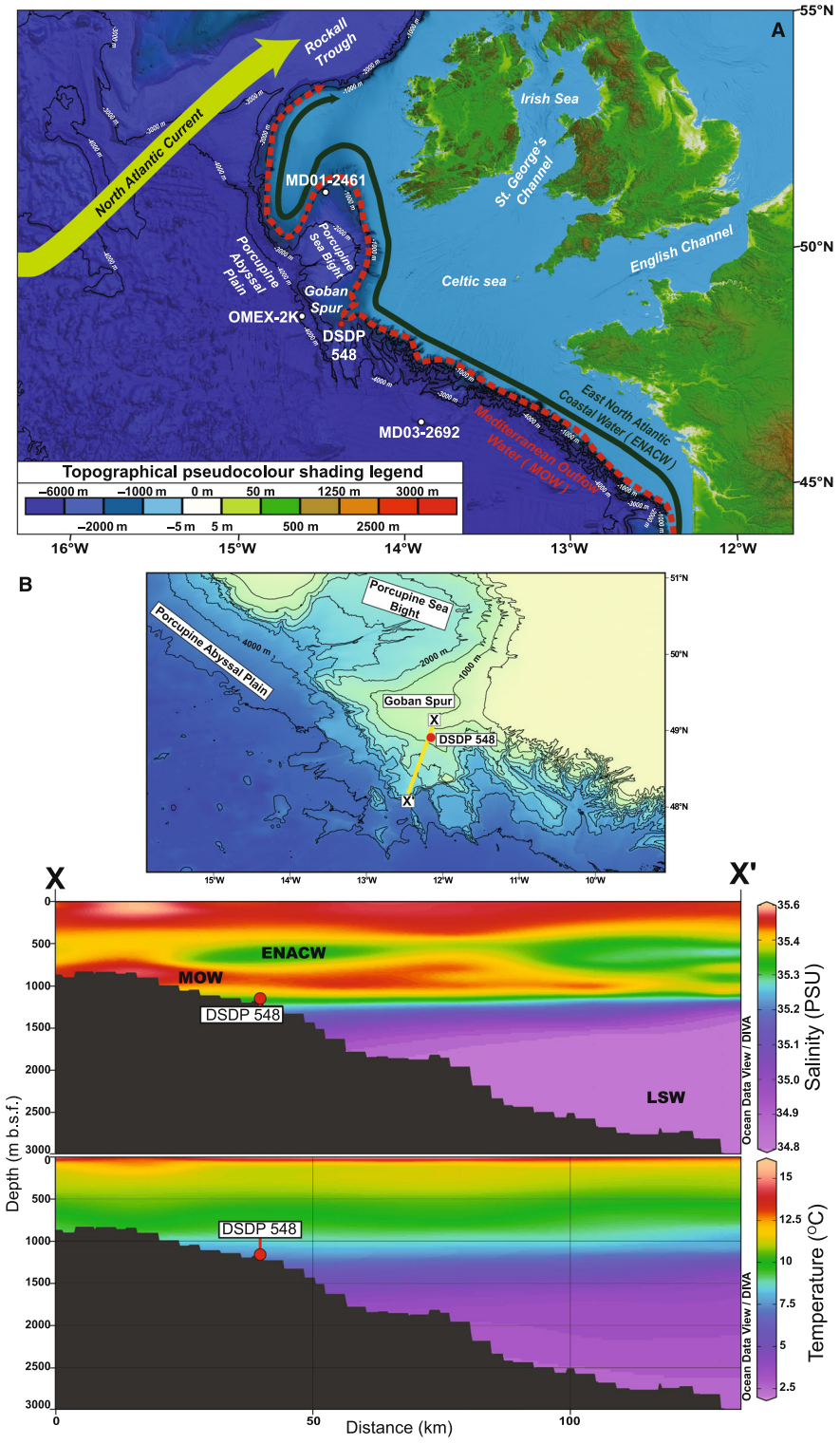

Fig. 4. A. The oceanic currents influencing the Goban Spur (Delivet *et al.* 2016) and the location of relevant cores: DSDP Site 548 (De Graciansky *et al.* 1985), IODP Site U1308 (Hodell *et al.* 2008), MD03-2692 (Toucanne *et al.* 2009), OMEX-2K (Haapaniemi *et al.* 2010) and MD01-2461 (Peck *et al.* 2007; Scourse *et al.* 2009). Each contour line denotes a 1000-m depth difference. B. Vertical salinity and temperature profile of those currents and the location of DSDP Site 548, modified after Delivet *et al.* (2016) using the Ocean Data View (ODV) software package of Schlitzer (2023). PSU = practical salinity unit; MOW = Mediterranean Outflow Water; ENACW = East North Atlantic Coastal Water; LSW = Labrador Sea Water. The black line marked with X and X' on the ends denotes the oceanographic profile line.

15023885, 0, Downloaded from https://onlinelibrary.wiley.com/doi/10.1111/bor.12631 by National Health And Medical Research Council, Wiley Online Library on [10/08/2023]. See the Terms and Conditions (https://onlinelibrary.wiley.com/terms-and-conditions) on Wiley Online Library for rules of use; OA articles are governed by the applicable Creative Commons License

water depth (m.w.d.) (Pingree & Le Cann 1990; Van Aken 2000; Delivet *et al.* 2016). MOW is more saline (35.6) and colder (9–10 °C), originating from the Bay of Biscay and flowing northward at ~800 m.w.d. (Delivet *et al.* 2016). Labrador Sea Water is a fresher (minimum salinity of 34.9) and colder (~5 °C) water-mass deeper than 1800 m.w.d. (Delivet *et al.* 2016).

DSDP Site 548 was cored during the DSDP Leg 80 in 1984 at 12°09.84′W at a water depth of 1256 m (Fig. 3A). The downhole wireline logging was conducted at Site 548A (48°54.93′N, 12°09.87′W), 30 m west of the cored section. This study focuses on the top 40 m of DSDP Core 548, consisting of alternations of Pleistocene to Holocene marly ooze and mud (Chennaux *et al.* 1985; De Graciansky *et al.* 1985). Preliminary biostratigraphy indicates a Pleistocene age for Unit 1 overlain by 28 cm of Holocene unlithified brown mud (De Graciansky *et al.* 1985).

Material and methods

Facies analyses

The facies of the 45 m DSDP Site 548 were logged and sampled for microfossils, lithic grains (IRD), and calcium carbonate content (%$CaCO_3$). The %$CaCO_3$ was measured on 89 samples using a modified volumetric technique of Huelsemann (1966) (cf. Wallace *et al.* 2002).

Foraminiferal analysis

Eighty-nine samples from DSDP Site 548 were dried, weighed, reacted with hydrogen peroxide, wet sieved using a 63-µm sieve, dried and split using a micro splitter for quantitative analysis. Approximately 150 to 200 planktonic foraminifera were counted in the >150 µm fraction, a size fraction typically used in palaeoceanographic studies (Kucera 2007).

We used Kucera's (2007) classification to identify planktonic foraminiferal assemblages based on their SST distribution and van Kreveld's (1996) classification to identify North Atlantic Current assemblages, which contains taxa from the sub-polar and transitional assemblages (Fig. 5A, Table 2).

Planktonic foraminiferal diversity is estimated using the criteria of Spellerberg & Fedor (2003), where the term 'diversity' refers to the number of species and individuals in each sample and not 'species richness', which commonly refers to the number of species observed in a population. Following the recommendation of Jost (2006), we use the effective number of species (ENS), calculated from the Shannon–Wiener index (Shannon 1948), as the measure of diversity.

We calculated diversity initially using the Shannon–Wiener index (Shannon 1948):

$$H = -\sum_{i=1}^{n} pi \ln pi \quad (1)$$

where H: Shannon–Wiener index, n: total number of species in a sample, and pi: proportion of individuals belonging to the i-th species.

Followed by conversion to ENS (Jost 2006):

$$ENS = \exp(H) \quad (2)$$

or:

$$ENS = \exp\left(-\sum_{i=1}^{n} pi \ln pi\right) \quad (3)$$

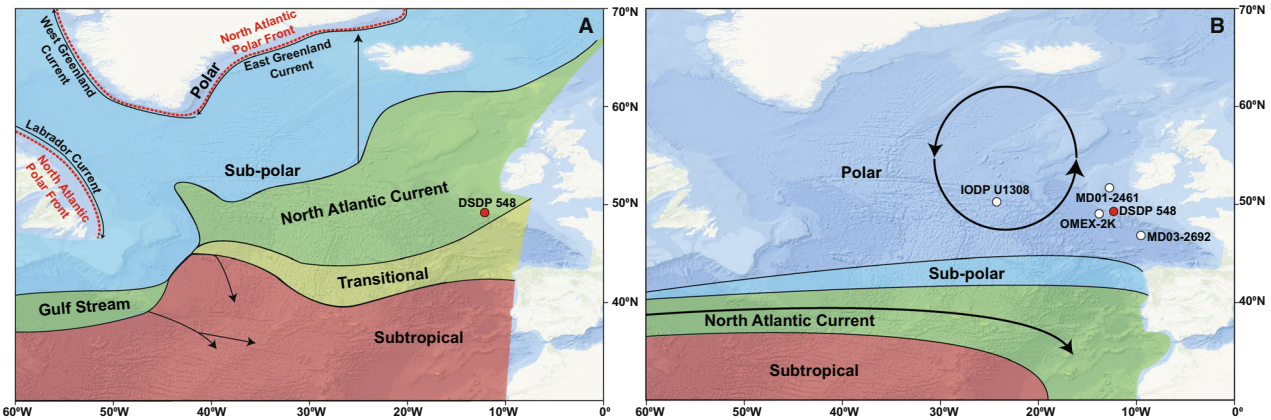

Fig. 5. A. Division of water-masses in the North Atlantic based on the planktonic foraminiferal assemblages, adapted from van Kreveld (1996); black arrows indicate the current direction. The present polar front location is adapted from Eynaud *et al.* (2009) and Barker *et al.* (2015). Red shading indicates subtropical water, yellow indicates transitional; green indicates North Atlantic Current water and light blue indicates sub-polar water. Polar water is the unshaded region north of the sub-polar water. B. Palaeoceanography of the North Atlantic during the Last Glacial Maximum, adapted from van Kreveld (1996), along with relevant core locations: DSDP Site 548 (De Graciansky *et al.* 1985), IODP Site U1308 (Hodell *et al.* 2008), MD03-2692 (Toucanne *et al.* 2009), OMEX-2K (Haapaniemi *et al.* 2010), and MD01-2461 (Peck *et al.* 2007; Scourse *et al.* 2009). Black arrows indicate the direction of surface currents.

15023885, 0, Downloaded from https://onlinelibrary.wiley.com/doi/10.1111/bor.12631 by National Health And Medical Research Council, Wiley Online Library on [10/08/2023]. See the Terms and Conditions (https://onlinelibrary.wiley.com/terms-and-conditions) on Wiley Online Library for rules of use; OA articles are governed by the applicable Creative Commons License

Table 2. Planktonic foraminifera grouping (van Kreveld 1996; Kucera 2007) and North Atlantic surface water-masses (Fig. 5).

Assemblage	Key species	Reference
Polar	*Neogloboquadrina pachyderma* (Ehrenberg, 1861)	Kucera (2007)
Sub-polar	*Neogloboquadrina incompta* (Cifelli, 1961)	
	Turborotalia quinqueloba (Natland, 1983)	
Transitional	*Globigerina bulloides* (d'Orbigny, 1826)	
	Globigerinita glutinata (Egger, 1893)	
	Globoconella inflata (d'Orbigny, 1839)	
	Globorotalia scitula (Brady, 1882)	
Subtropical	*Beela digitata* (Brady, 1879)	
	Globigerina falconensis (Blow, 1959)	
	Globigerinella calida (Parker, 1962)	
	Globigerinella siphonifera (d'Orbigny, 1839)	
	Globigerinoides conglobatus (Brady, 1879)	
	Globigerinoides ruber (d'Orbigny, 1839) subsp. *albus* (Morard *et al*., 2019)	
	Globorotalia hirsuta (d'Orbigny, 1839)	
	Globorotalia truncatulinoides (d'Orbigny, 1839)	
	Globoturborotalia rubescens (Hofker, 1956)	
	Globoturborotalia tenellus (Parker, 1958)	
	Neogloboquadrina dutertrei (d'Orbigny, 1839)	
	Orbulina universa (d'Orbigny, 1839)	
Tropical	*Globigerinoides ruber* subsp. *ruber* (d'Orbigny, 1839)	
	Globorotalia crassaformis (Galloway & Wissler, 1927)	
	Globorotalia menardii (d'Orbigny in Parker, Jones & Brady, 1865)	
	Pulleniantina obliquiloculata (Parker & Jones, 1865)	
	Sphaeroidinella dehiscens (Parker & Jones, 1865)	
	Trilobatus sacculifer (Brady, 1877)	
North Atlantic Current	*Globigerina bulloides* (d'Orbigny, 1826)	Van Kreveld (1996)
	Neogloboquadrina incompta (Cifelli, 1961)	
	Globorotalia scitula (Brady, 1882)	
	Globigerinita glutinata (Egger, 1893)	
	Globoconella inflata (d'Orbigny, 1839)	

where *ENS*: effective number of species, *H*: Shannon–Wiener index, *n*: total number of species in a sample, and *pi*: proportion of individuals belonging to the *i*-th species.

Lithic grain/ice rafted debris (IRD) analyses

A lithic grain census was carried out on an aliquot of the microfossil residue. Lithic concentration is expressed as the number of IRD per gram of dried sediment. The lithic grains were counted in the >250 and >150 μm size fractions. The >250 μm fraction was counted to determine the stratigraphical distribution of IRD, as the grains in this size fraction are not likely to be transported to DSDP Site 548 by means other than calving icebergs due to their size and weight.

Splits of microfossil residue with a minimum of 200 counts of lithic grains were also counted in the >150 μm size fraction. The >150 μm size fraction is typically counted for IRD lithic analyses in the northwest Atlantic (Andrews 2000; Peck *et al*. 2007; Scourse *et al*. 2009). The 150 μm lithics were classified using the Peck *et al*. (2007) classification (Table 3) and can be divided into clear quartz, stained quartz, 'Heinrich-layer'-related, BIIS-related, and volcanic grains. Unidentified lithic grains with multiple possible origins were classified as 'other'.

Benthic foraminifera stable isotope analysis

Carbon and oxygen isotope ($\delta^{13}C$ and $\delta^{18}O$) measurements on the benthic foraminifera taxa *Cibicides* spp., *Cibicidoides* spp., *Cassidulina laevigata* and *Bullimina* spp. were carried out at the Institute of Geology and Palaeontology at the University of Münster (Germany) using a GasBench connected to a ThermoScientific Delta V Plus mass spectrometer via a ConFlo III interface. Individual measurements were carried out on sonicated foraminiferal tests, with sample weights between 50 and 180 μg per analysis. Results are reported in the standard delta notation as per mil difference relative to V-PDB (Vienna Pee Dee Belemnite). Accuracy was checked against two in-house standards, as well as against NBS-19. Reproducibility, as determined through replicate measurements of standards that were not used for the correction scheme, was better than ±0.16‰ for $\delta^{18}O$ and ±0.06‰ for $\delta^{13}C$ (2σ).

Results

Age model

The new age model for the top 40 m of DSDP Site 548 is principally based on the correlation of multispecies benthic oxygen isotope ratio, including *Cibicides* spp.,

15023885, 0, Downloaded from https://onlinelibrary.wiley.com/doi/10.1111/bor.12631 by National Health And Medical Research Council, Wiley Online Library on [10/08/2023]. See the Terms and Conditions (https://onlinelibrary.wiley.com/terms-and-conditions) on Wiley Online Library for rules of use; OA articles are governed by the applicable Creative Commons License

Table 3. IRD lithic grain classification for the Porcupine Sea Bight adapted from Peck *et al.* (2007).

Assemblage	Type	Proposed origins	Reference	Ice sheet designation
Heinrich layer	Dolomitic carbonate	Hudson Bay	Bond *et al.* (1992)	LIS
		Ellesmere Island	Nørgaard-Pedersen *et al.* (2007)	
	Hornblende	North American igneous province	Hemming *et al.* (1998)	LIS
		NW Scotland	Peck *et al.* (2007)	BIIS
	Haematite coated grains	Gulf of St. Lawrence	Bond & Lotti (1995)	LIS
		Eastern Greenland	van Kreveld *et al.* (2000)	East Greenland ice sheet
		British Isles	Peck *et al.* (2007)	BIIS
BIIS	Limestone	Carboniferous formations of Ireland	Knutz *et al.* (2001)	BIIS
	Shale			
	Black limestone			
	Chalk	Irish Sea ice stream	Scourse *et al.* (2000)	BIIS
	Schist/mica	Scottish metamorphic provinces	Peck *et al.* (2007)	BIIS
Volcanic	Obsidian	Icelandic obsidian province	Bond & Lotti (1995)	Icelandic ice sheet
	Basalt			
	Pumice	Tertiary volcanic province of NW British Isles	Knutz *et al.* (2001)	BIIS
	Tephra	Icelandic eruptions	Lacasse *et al.* (1996)	Icelandic ice sheet

Cibicidoides spp., *Cassidulina laevigata* and *Bullimina* spp., to the LR04 benthic oxygen isotope stack of Lisiecki & Raymo (2005) (Fig. 6) guided by initial age bracketing using wireline NGR measurements from DSDP Site 548-A (Fig. S1), and DSDP 548's %NPS (*Neogloboquadrina pachyderma* relative abundance), and %$CaCO_3$ content (Figs S2, S3). Multispecies benthic oxygen isotope correlation is employed to create a continuous record despite some intervals' low benthic foraminifera yield in DSDP Core 548. We acknowledge species-specific vital effects cause significant variance in foraminiferal stable isotope composition (cf. Ravelo & Hillaire-Marcel 2007). However, careful considerations and analysis of the general down-core variations of benthic oxygen isotope, supplemented by other climatic proxies and comparison to other data sets, can still yield a useful age model. Some peaks of IRD and %NPS horizons, such as at 6 and 10.5 m b.s.f. (85% NPS, 1828 lithic clasts/gram dried sediment and 84% NPS, 818 lithic clasts/gram dried sediment, respectively) showed anomalously light oxygen isotope values (Fig. 6) interpreted to represent freshwater influx due to increased iceberg calving; hence those were not used to construct the age model. An attached Supporting Information file contains a detailed explanation of the age model (Data S1).

Additional datums for our age model were obtained by correlating %NPS trends to MD03-2692 (Mojtahid *et al.* 2005) in the northern part of the Bay of Biscay, 320 km southeast of the Goban Spur (Figs 1, S4). The tie points used to constrain the age are in Table 4. The age model for the studied interval and its linear sedimentation rate are then derived by linearly extrapolating the tie points (Fig. S5). Comparison to the data sets from ODP 983 (Barker *et al.* 2019), MD01-2461 (Peck *et al.* 2007) and MD03-2692 (Mojtahid *et al.* 2005) (Fig. S6) shows that the age model for DSDP 548 conforms well with regional trends.

Facies and physical property variability

Four alternating facies are present in the top 45 m at DSDP Site 548, organic-rich mud, calcareous mud, calcareous silt, and calcareous silty sand (Figs 7A, 8). Bedding contact between these lithofacies is gradational or sharp and often bioturbated (Figs 7B, 9). Bioturbation features include ellipsoids and vertical and horizontal burrows infilled with adjacent facies (Fig. 7B). Occasional mud intervals are weakly laminated with large (up to 2 cm in diameter) lithic clasts (Figs 7A, 9). The %$CaCO_3$ positively correlates with sediment grain size,

15023885, 0, Downloaded from https://onlinelibrary.wiley.com/doi/10.1111/bor.12631 by National Health And Medical Research Council, Wiley Online Library on [10/08/2023]. See the Terms and Conditions (https://onlinelibrary.wiley.com/terms-and-conditions) on Wiley Online Library for rules of use; OA articles are governed by the applicable Creative Commons License

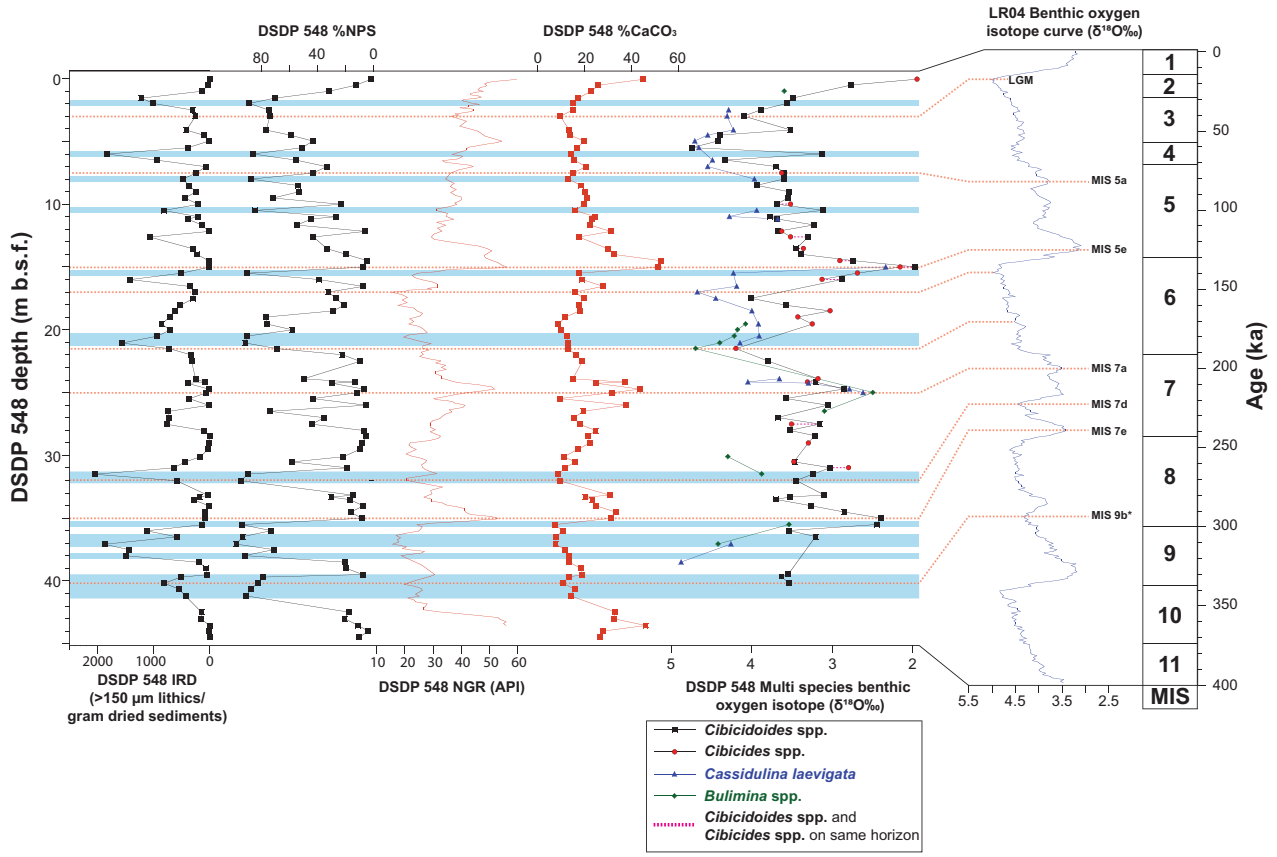

Fig. 6. The correlation between the relative abundance of *Neogloboquadrina pachyderma* (%NPS), %$CaCO_3$, NGR (De Graciansky *et al.* 1985) at DSDP Site 548 and the LR04 stack of Lisiecki & Raymo (2005). Light blue shading indicates intervals with ≥80% NPS, interpreted to signify the presence of the polar front at or south of DSDP Site 548. Red dashed lines indicate the correlative horizons. m b.s.f. = metres below sea floor; API = American Petroleum Institute (a unit for natural gamma radiation).

Table 4. Tie points for the age model correlation to LR04 benthic oxygen isotope curve of Lisiecki & Raymo (2005) and %NPS of MD03-2692 of Mojtahid *et al.* (2005).

Core depth (m b.s.f.)	Note	Age (ka)	Source	Reference
0.28	The base of Holocene mud	11.65	DSDP 548 initial report	De Graciansky *et al.* (1985)
3.00	LGM	18	LR04 benthic oxygen isotope	Lisiecki & Raymo (2005); Railsback *et al.* (2015)
7.52	MIS 5a	82		
15.02	MIS 5e	125		
17.00	MIS 6	140		
21.06	%NPS peak	155.2	MD03-2692	Mojtahid *et al.* (2005)
21.50	MIS 6	171	LR04 benthic oxygen isotope	Lisiecki & Raymo (2005); Railsback *et al.* (2015)
25.02	MIS 7a	200		
32.02	MIS 7d	223		
35.02	MIS 7e	240		
36.49	%NPS peak	263	MD03-2692	Mojtahid *et al.* (2005)
39.50	%NPS trough	283		
40.19	MIS 9	294	LR04 benthic oxygen isotope	Lisiecki & Raymo (2005); Railsback *et al.* (2015)

ranging from a minimum of 5% in the mud to 65% in the silt/sand facies (Fig. 8). %$CaCO_3$ in the mud reaches a maximum of 30%, whereas, in the calcareous silt, it varies from 30 to 50% and 40 to 50% in the silty sand. The organic-rich mud facies (Fig. 7A) typically yield abundant %NPS, IRD and elevated NGR values with low

15023885, 0, Downloaded from https://onlinelibrary.wiley.com/doi/10.1111/bor.12631 by National Health And Medical Research Council, Wiley Online Library on [10/08/2023]. See the Terms and Conditions (https://onlinelibrary.wiley.com/terms-and-conditions) on Wiley Online Library for rules of use; OA articles are governed by the applicable Creative Commons License

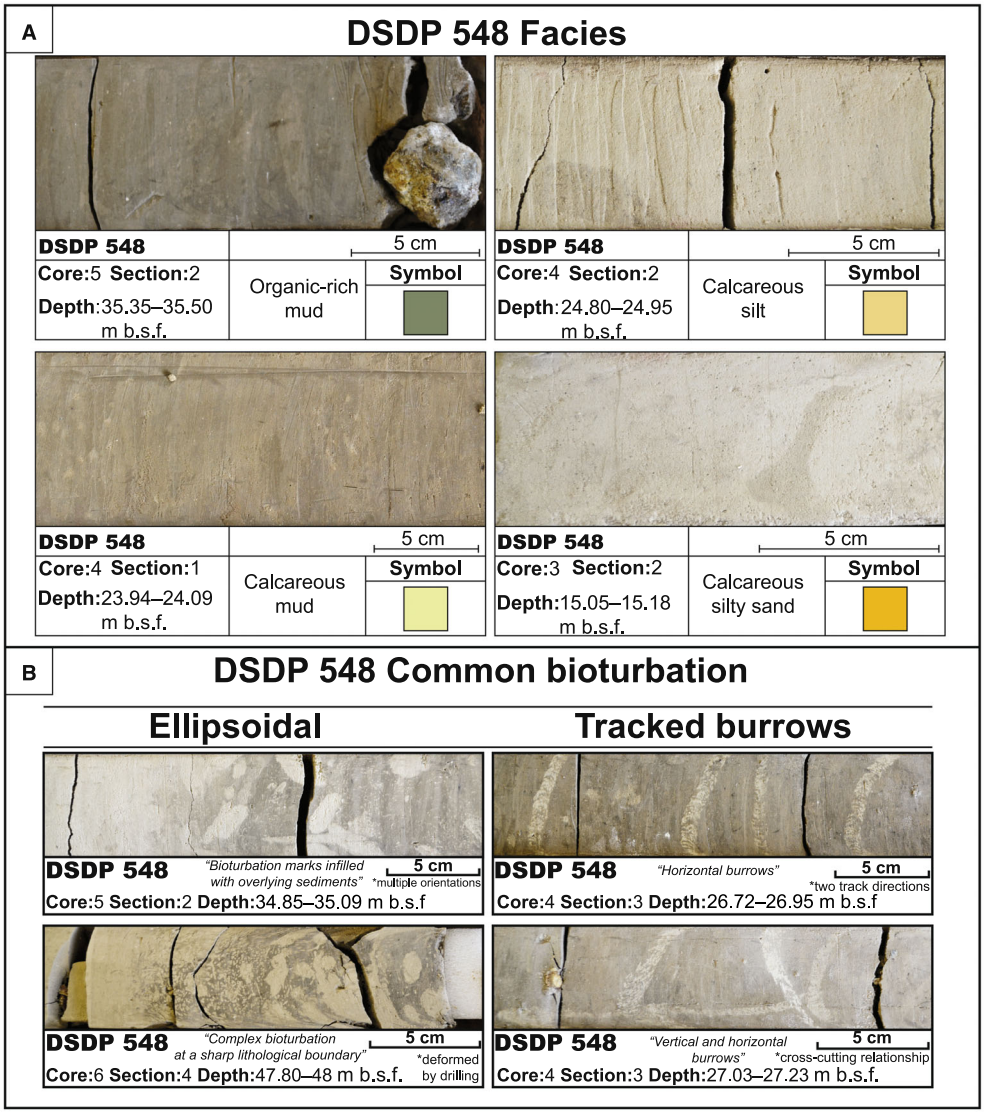

Fig. 7. A. Four types of facies in the upper 45 m at DSDP Site 548. B. Common bioturbation marks in the studied interval. The upper section of the core is on the left side of each image.

diversity planktonic foraminiferal assemblages (Fig. 9). In contrast, calcareous silty sand facies (Fig. 7A) are characterized by minor %NPS and IRD, low NGR values and high planktonic foraminiferal diversity and abundance and are associated with warmer interglacial intervals (Fig. 8).

Lithic grain distribution

The down-core lithic variability between the >150 and >250 μm fractions is similar (Fig. 10), and lithic grain abundance shows a strong positive correlation to %NPS (Fig. 11), suggesting a significant increase of both size fractions during the colder periods. Lithic grain assemblage in the >150 μm fractions is dominated by clear quartz, which makes up 65 to 75% of the total clasts (Fig. 10). The next most common grain type is stained quartz grains, with colours ranging from yellow to reddish-orange and occasionally light pink due to iron oxide staining. Other common lithic grains include mica schist, vesicular basalt and obsidian, rhyolitic tuff, granite and granodiorite, grey shale, chalk, and dark grey to light cream-coloured carbonates.

BIIS lithics dominate IRD maxima, except at ~14.6 ka, where volcanic clasts are common. The Heinrich lithics are a minor component of some IRD-rich horizons, such as at 60 and ~33 ka, corresponding to HE 6 and 3 (Fig. 10). Heinrich lithics are rare, making up less than ~2% of all lithics, suggesting minor LIS-sourced IRD at Site 548. The absolute abundance of the LIS-sourced IRD at the Goban Spur is less than at OMEX-2K (Haapaniemi *et al.* 2010) or MD01-2461 (Peck *et al.* 2007).

15023885, 0, Downloaded from https://onlinelibrary.wiley.com/doi/10.1111/bor.12631 by National Health And Medical Research Council, Wiley Online Library on [10/08/2023]. See the Terms and Conditions (https://onlinelibrary.wiley.com/terms-and-conditions) on Wiley Online Library for rules of use; OA articles are governed by the applicable Creative Commons License

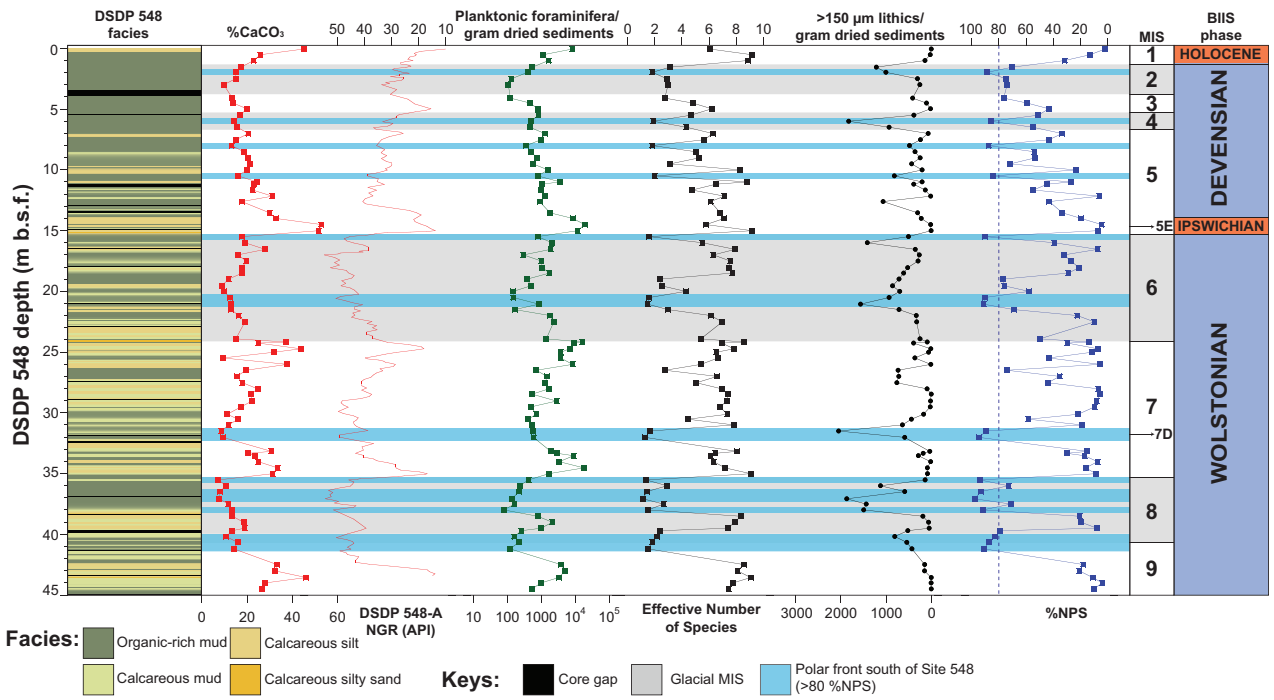

Fig. 8. Facies, %$CaCO_3$, lithic grain concentration, foraminiferal diversity and concentration at Site 548. The natural gamma radiation (NGR) values at DSDP Site 548-A (De Graciansky *et al.* 1985). MIS classification is based on Lisiecki & Raymo (2005) and Railsback *et al.* (2015). BIIS phases are from Van Rooij *et al.* (2006) and Thierens *et al.* (2012). API = American Petroleum Institute (a unit for natural gamma radiation). The orange bar in the rightmost column denotes the interglacial interval bounding the BIIS phases.

The Wolstonian BIIS glacial shows two IRD maxima near the start and end (~265 and 252 ka during MIS 8 and ~155 and 132 ka during MIS 6; Fig. 10). In addition, an IRD maximum is at ~221 ka during the MIS 7d stadial. IRD maxima at ~252, 221 and 132 ka correlate to Terminations 3, 3A and 2. During the Devensian phase, several IRD peaks are equivalent to HE 3, 6 and 1 and the final phase of the last BIIS at ~14.6 ka (Fig. 10). However, the sampling density in this interval is insufficient to determine the nature of other Heinrich Events (HE 5, 4 and 2).

Planktonic foraminiferal assemblages

The planktonic foraminiferal assemblage is dominated by the polar species *Neogloboquadrina pachyderma* (sinistral), with lesser amounts of sub-polar and transitional taxa such as *Neogloboquadrina incompta*, *Globigerina bulloides*, *Globoconella inflata* and *Turborotalia quinqueloba* (cf. van Kreveld 1996; Kucera 2007). Occasional incursions of subtropical planktonic species such as *Orbulina universa*, *Neogloboquadrina dutertrei* and *Globorotalia truncatulinoides* occur in interglacials (MIS 7, 5 and 1; Fig. 12). These subtropical taxa typify calcareous sandy-silty facies with minimal lithics and elevated planktonic foraminifera abundance and diversity (Fig. 8). %NPS varies from 98% to a minimum of 2%. Intervals with >80%NPS are common during the glacial MIS and stadial periods within interglacial MIS, such as those at MIS 7 and 5; %$CaCO_3$ poor mud facies rich in lithic grains characterize these low planktonic foraminiferal abundance and diversity horizons (Fig. 8). The detailed >150 µm planktonic foraminifera counts from the top 45 m of DSDP 548 are listed in Data S2.

Interpretation and discussion

The glacial–interglacial sedimentation at the Goban Spur

Presently, the most active bottom current at Site 548 is the MOW (Fig. 4A, B). MOW intensity varied over the last ~130 000 years (Kaboth *et al.* 2017), with stronger MOW regimes during the interglacial periods. The alternations of calcareous silty sand contourites (Fig. 9) with warmer water planktonic foraminifera (Fig. 12) during interglacial periods and glacial mud pelagites with abundant cold water species (Fig. 8) at Site 548 suggests that this glacial/interglacial modulation of relative MOW intensity extended back to at least 250 000 years ago.

Lithics and IRD at the Goban Spur

The strong positive correlation between lithic grain abundance of both size fractions and %NPS (Fig. 11) suggests that the lithic clasts in the uppermost 40 m of DSDP Core 548 are associated with glacial periods. The lack of submarine channels and canyons affecting

15023885, 0, Downloaded from https://onlinelibrary.wiley.com/doi/10.1111/bor.12631 by National Health And Medical Research Council, Wiley Online Library on [10/08/2023]. See the Terms and Conditions (https://onlinelibrary.wiley.com/terms-and-conditions) on Wiley Online Library for rules of use; OA articles are governed by the applicable Creative Commons License

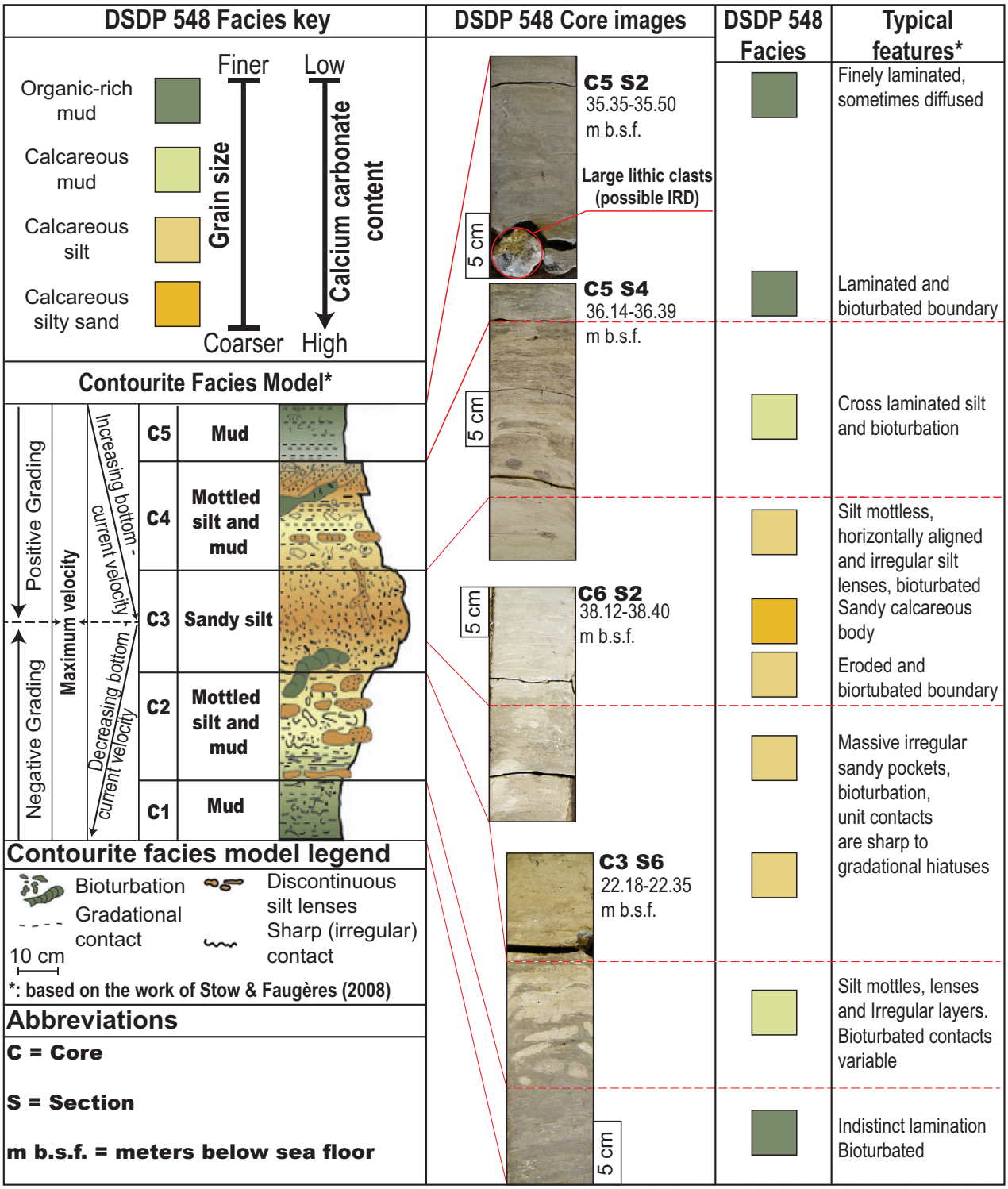

Fig. 9. Examples of the contourite facies at DSDP Site 548 following the classification of Stow & Faugères (2008).

the down-slope glacial sedimentation at the Goban Spur (Fig. 3B) suggests that these glacial lithic clasts are related to iceberg calving. The relative rarity of Hudson Bay-related lithics and the dominance of the BIIS lithics (Fig. 10) in IRD-rich mud horizons (Fig. 8) suggest that they were mainly sourced from the BIIS. The two Heinrich Event (HE 6 and 1) equivalent horizons sampled in the uppermost section are characterized by abundant IRD, >80%NPS, and low planktonic foraminifera productivity and species diversity. In

15023885, 0, Downloaded from https://onlinelibrary.wiley.com/doi/10.1111/bor.12631 by National Health And Medical Research Council, Wiley Online Library on [10/08/2023]. See the Terms and Conditions (https://onlinelibrary.wiley.com/terms-and-conditions) on Wiley Online Library for rules of use; OA articles are governed by the applicable Creative Commons License

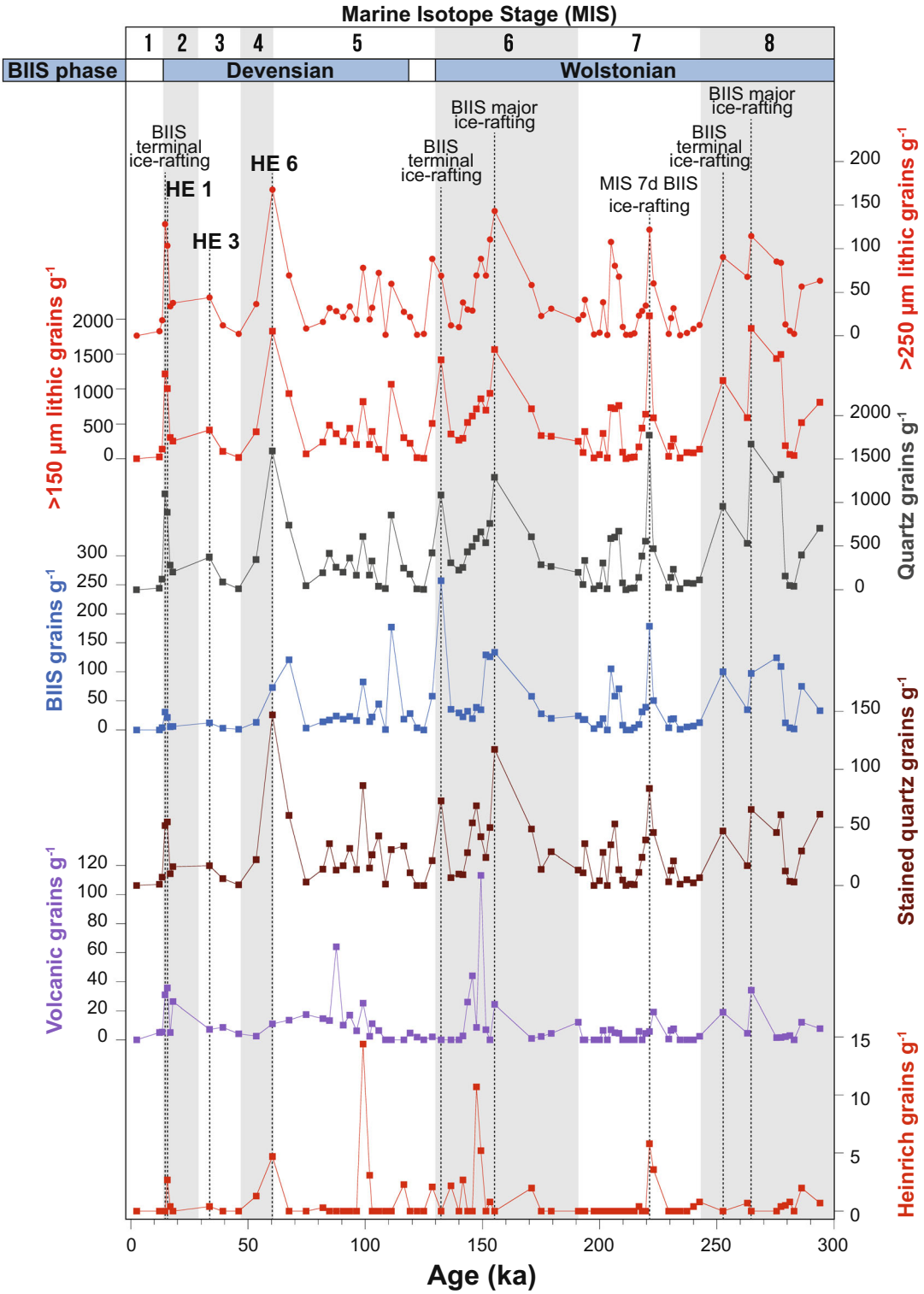

Fig. 10. The abundance of lithics at Site 548 based on the classification of Peck *et al.* (2007). All the lithic grain groupings are from the >150 µm size fraction.

comparison, the HE 3 equivalent horizon is marked by a slight increase in IRD and below polar level %NPS (Fig. 13).

At IODP Site U1308, IRD-rich horizons are typically characterized by high Si/Sr ratios, and Heinrich Event IRDs from Hudson Bay have high Ca/Sr ratios due to the

15023885, 0, Downloaded from https://onlinelibrary.wiley.com/doi/10.1111/bor.12631 by National Health And Medical Research Council, Wiley Online Library on [10/08/2023]. See the Terms and Conditions (https://onlinelibrary.wiley.com/terms-and-conditions) on Wiley Online Library for rules of use; OA articles are governed by the applicable Creative Commons License

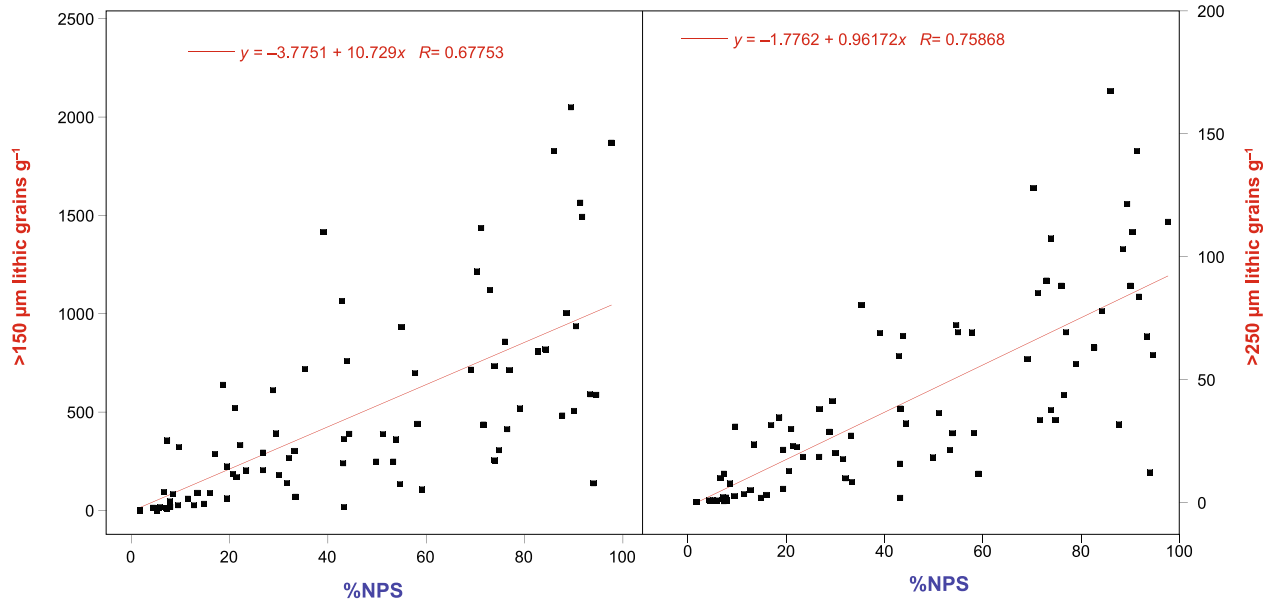

Fig. 11. Correlation between the >150 and >250 µm fraction lithic concentration and %NPS.

abundance of detrital carbonate (Hodell *et al.* 2008). Thus, high Ca/Sr and Si/Sr ratios at IODP Site U1308 indicate increased IRD deposition from the LIS. Hodell *et al.* (2008) used these ratios to identify Heinrich Events in the mid-latitude Central Atlantic. Thus, by comparing the Si/Sr and Ca/Sr ratios at Site U1308 and the %NPS and IRD concentration at Site 548 and MD03-2692 (Fig. 13), it is possible to relate IRD events at Site 548 to LIS discharge, BIIS discharge, or other northwest European ice-sheet discharge. This relationship is essential during stadial periods as the westward flowing North Atlantic Current was not present north of 45°N, and the oceanography of the region was dominated by polar water (van Kreveld 1996; Fig. 5B); this allowed icebergs from northwest European ice sheets to travel westwards to the central Atlantic Ocean.

We characterize IRD maxima with abundant %NPS horizons at Site 548 based on their association with MIS termination events (Tables 5, 6). We suggest IRD maxima not associated with MIS terminations could represent cold periods when ice shelves were forming around the BIIS (Batchelor *et al.* 2019), and their subsequent calving may relate to factors such as glacial-isostatic adjustment related to sea level change (Bradley *et al.* 2023) or megatides (Scourse *et al.* 2018). In comparison, IRD maxima at terminations represent the intense iceberg-calving episodes associated with the waning of the BIIS with the onset of interglacial climate.

Polar front and BIIS discharge history at the Goban Spur

This section outlines 250 000 years of the polar front and BIIS iceberg discharge history at the Goban Spur. We follow the BIIS chronology of Hughes *et al.* (2022) and Clark *et al.* (2022), the MIS chronology of Lisiecki & Raymo (2005), where evenly numbered MIS correspond to colder periods, and odd numbers indicate warmer periods along with the standardized marine isotope substages naming convention of Railsback *et al.* (2015). In addition, we also use stage names specific to the British Isles for each MIS (Table 1). Our results are then compared to MD03-2692 (Figs 1, 13) to determine the polar front history of the Celtic Margin.

Marine Isotope Stage 8 (Middle Wolstonian BIIS). – The polar front was south of the Goban Spur at ~277 ka, from ~265 to ~263 ka, and at ~243 ka, with IRD peaks at ~277, ~265 and ~253 ka. These IRD maxima correlate to periods with high Si/Sr and low Ca/Sr ratios at IODP Site 1308 (Hodell *et al.* 2008; Fig. 13), suggesting increased IRD input to the North Atlantic from sources other than the LIS, possibly the northwest European ice sheet. The ~265 ka IRD peak has an equivalent at MD03-2692 in the Bay of Biscay (Mojtahid *et al.* 2005), interpreted to represent the BIIS maximum during MIS 8, equivalent to the Fennoscandian Ice Sheet maximum extent (Olsen *et al.* 2013). Subsequently, the BIIS disintegrated rapidly during Termination 3 following the terminal ice rafting event at ~252 ka.

The migration of the polar front south of the Goban Spur at ~243 ka is atypical as it does not coincide with significant IRD deposition at the Goban Spur or MD03-2692 in the Bay of Biscay (Mojtahid *et al.* 2005; Fig. 13). This event was relatively short-lived as, ~3000 years later, the %NPS fell from ~94 to ~9%, equivalent to a sea surface temperature (SST) increase of >5 °C (Govin

15023885, 0, Downloaded from https://onlinelibrary.wiley.com/doi/10.1111/bor.12631 by National Health And Medical Research Council, Wiley Online Library on [10/08/2023]. See the Terms and Conditions (https://onlinelibrary.wiley.com/terms-and-conditions) on Wiley Online Library for rules of use; OA articles are governed by the applicable Creative Commons License

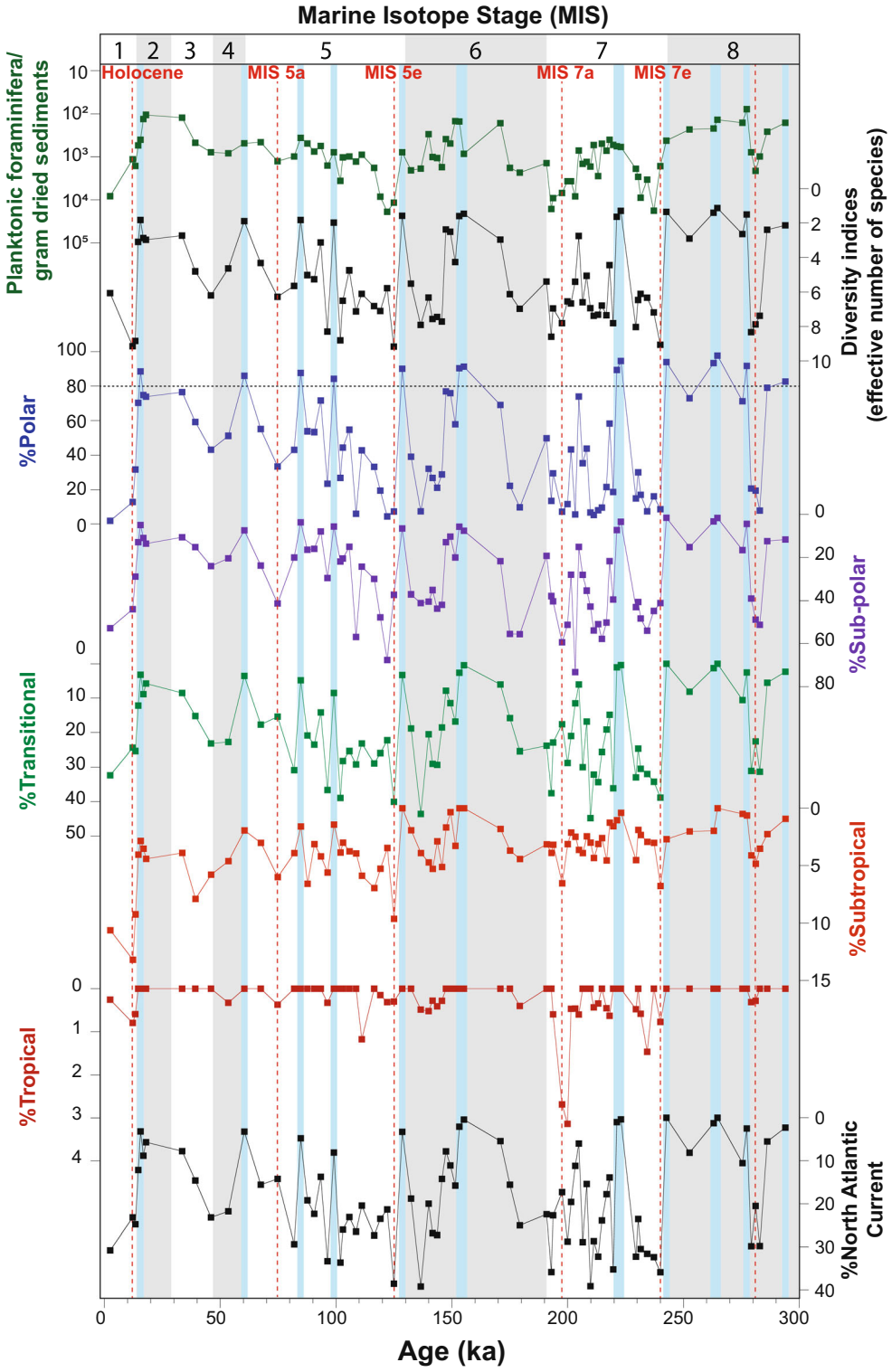

Fig. 12. Major planktonic foraminiferal group distribution at DSDP Site 548. Planktonic foraminifera grouping is based on van Kreveld (1996), and diversity calculation is based on the work of Jost (2006). Red dashed vertical lines highlight subtropical and tropical planktonic foraminifera influx to the Goban Spur.

et al. 2012). This end MIS 8 cold interval was possibly too short-lived for the BIIS to expand sufficiently to shed IRD-bearing icebergs into the Goban Spur and the Bay of Biscay. However, at IODP Site U1308, equivalent Si/Sr and Ca/Sr ratio maxima (Hodell *et al.* 2008) suggest increased IRD deposition from the LIS into the central

15023885, 0, Downloaded from https://onlinelibrary.wiley.com/doi/10.1111/bor.12631 by National Health And Medical Research Council, Wiley Online Library on [10/08/2023]. See the Terms and Conditions (https://onlinelibrary.wiley.com/terms-and-conditions) on Wiley Online Library for rules of use; OA articles are governed by the applicable Creative Commons License

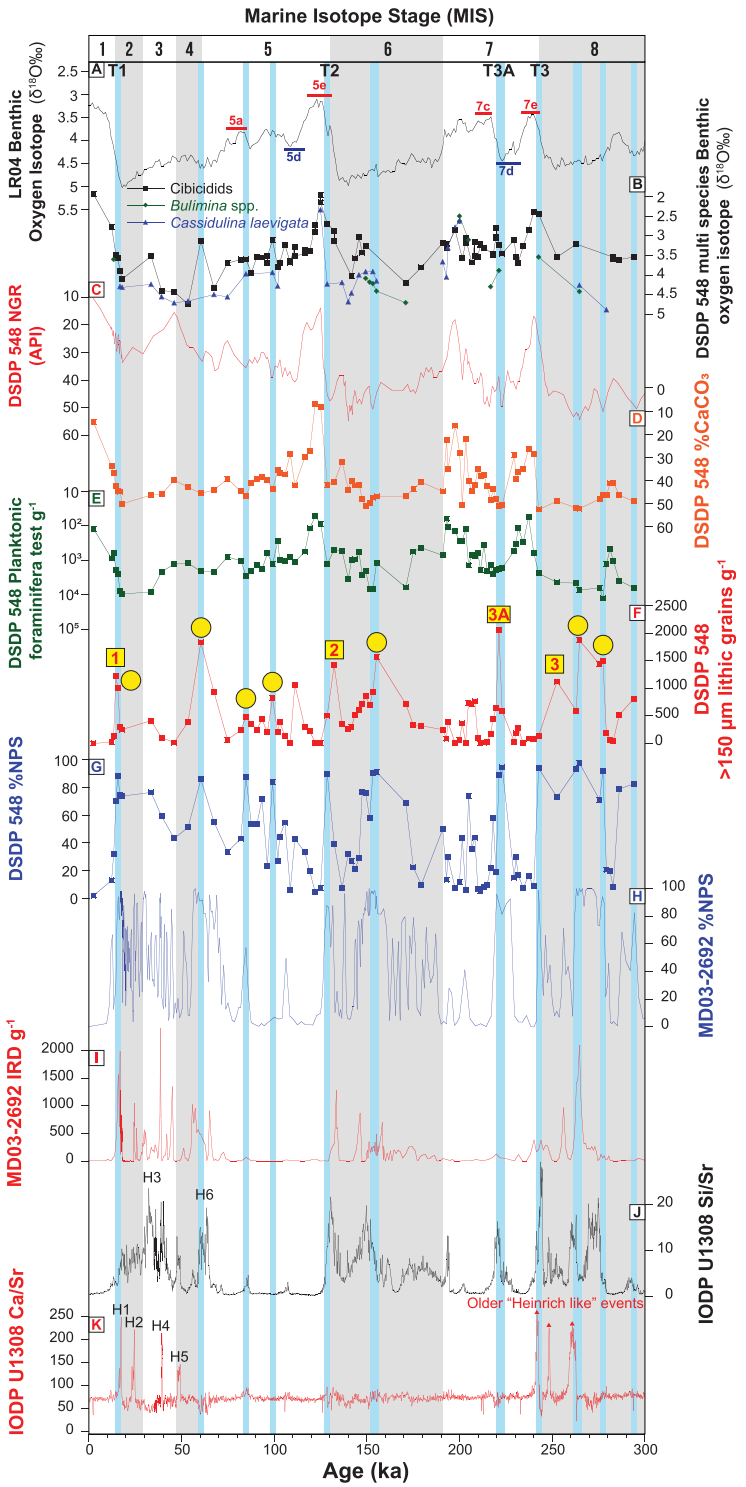

Fig. 13. A comparison of data from DSDP Site 548 with MD03-2692 and IODP Site U1308. A. LR04 benthic oxygen isotope stack (Lisiecki & Raymo 2005). B. DSDP 548 Multispecies benthic oxygen isotope curve. C. DSDP 548 natural gamma radiation, depth converted from the measurement at DSDP 548-A (Fig. S1; De Graciansky *et al.* 1985). API = American Petroleum Institute (a unit for natural gamma radiation). D. DSDP 548 %$CaCO_3$. E. DSDP 548 planktonic foraminiferal abundance. F. DSDP 548 ice rafted debris (counts/gram dried sediments). G. DSDP 548 %NPS (this work). H. MD03-2692 %NPS. I. MD03-2692 ice rafted debris (counts/gram dried sediments) (Mojtahid *et al.* 2005). J. IODP Site U1308 Si/Sr ratio. K. IODP Site U1308 Ca/Sr ratio (Hodell *et al.* 2008). Yellow circles and blue shading indicate periods when the polar front was south of Site 548, associated with IRD maxima. Yellow squares indicate high IRD and %NPS horizons associated with MIS terminations. The termination events are in red. Grey shading indicates glacial MIS. Red bars around the LR04 curve indicate interstadial intervals, and dark blue bars indicate stadial intervals (Railsback *et al.* 2015).

15023885, 0, Downloaded from https://onlinelibrary.wiley.com/doi/10.1111/bor.12631 by National Health And Medical Research Council, Wiley Online Library on [10/08/2023]. See the Terms and Conditions (https://onlinelibrary.wiley.com/terms-and-conditions) on Wiley Online Library for rules of use; OA articles are governed by the applicable Creative Commons License

Table 5. List of peak IRD horizons at DSDP 548 with abundant NPS not associated with MIS terminations. Note that HE 2, 4 and 5 were not documented due to insufficient sampling resolution in the upper part of the core, whereas HE 3 is marked with lower than 80% NPS.

Age (ka)	% NPS	IRD concentration (grains g^{-1})	BIIS phase	Event	Notes
15.5	88	1004	Devensian	HE 1	BIIS/IIS major calving event
60	86	1828		HE 6	End of MIS 4
155	91	1565	Wolstonian	End of Drenthe glacial advance	Middle MIS 6 BIIS discharge
265	98	1870			Middle MIS 8 BIIS discharge
277	92	1494			

North Atlantic during an 'older' Heinrich-like event late in MIS 8.

Marine Isotope Stage 7. – Compared to MIS 8, initial MIS 7 conditions at the Goban Spur were warmer. The relative absence of IRD suggests a restricted BIIS, which reached its minimum by ~234 ka, along with the onset of interstadial conditions by MIS 7e (Fig. 13). However, the interstadial climate did not persist throughout MIS 7 as the polar front migrated south of the Goban Spur by ~223 ka, associated with an IRD peak at ~221 ka (Fig. 13), suggesting glacial conditions and an actively calving BIIS during the MIS 7d stadial. At MD03-2692, MIS 7d was marked by the influx of the cold water dinoflagellates such as *Spiniferites elongatus* and *Spiniferites septentrionalis* (Penaud *et al.* 2008) with %NPS maxima (Mojtahid *et al.* 2005), suggesting cooling in the Bay of Biscay. During this time, the pollen record from offshore Portugal (Roucoux *et al.* 2006) shows a significant reduction in tree density and steppe vegetation expansion, typical continental European interstadial dry and cold climates. However, the ~221 ka IRD peak at Goban Spur is not present at MD03-2692 (Mojtahid *et al.* 2005), although an equivalent horizon occurs at IODP Site U1308, marked with high Si/Sr and low Ca/Sr ratio indicating increased IRD deposition from the northwest European ice sheet (Hodell *et al.* 2008) (Fig. 13). We suggest this variability represents significant calving events from the BIIS to the Goban Spur associated with an episode of rapid expansion during MIS 7d followed by its abrupt collapse by Termination 3A.

IRD and %NPS are rare in the Goban Spur and Bay of Biscay during the interstadial MIS 7c, suggesting warmer conditions at ~212 ka. This period is associated with the influx of the interglacial climatic optimum indicator dinoflagellate taxon *Spiniferites mirabilis* at MD03-2692 (Penaud *et al.* 2008), while pollen records from northeastern Greece suggest a diverse forest flora during MIS 7c (Tzedakis *et al.* 2003). We suggest the Wolstonian BIIS was actively calving during the MIS 7d stadial with a terminal ice rafting episode associated with Termination 3A. In addition, this event is bounded by two episodes of significant reduction of IRD deposition at Site 548 during the interstadial climate of MIS 7e and MIS 7c (Fig. 13).

Marine Isotope Stage 6 (Late Wolstonian BIIS). – The polar front was at or south of Site 548 at ~152 and ~155 ka during MIS 6. IRD deposition at the Goban Spur reached its maximum by ~155 ka associated with MIS 6 BIIS expansion (Fig. 13), contemporaneous with the Netherlands' Drenthe glacial advance (Gibbard *et al.* 2022). Toucanne *et al.* (2009) interpreted enhanced 'Fleuve Manche' fluvial activity east of the Bay of Biscay at ~155 ka to be related to increased western European ice sheets' discharge intensity. High Si/Sr and low Ca/Sr ratios from equivalent horizons at IODP Site U1308 (Hodell *et al.* 2008; Fig. 13) suggest increased non-LIS IRD deposition to the region. Those observations suggest that during the coldest phase of MIS 6, the BIIS actively shed sediments into Britain's 'Fleuve Manche' tributary rivers while also discharging IRD-bearing icebergs westwards into the central North Atlantic.

Subsequently, transitional species such as *Globigerina bulloides* dominated the planktonic foraminiferal assemblages at Site 548, associated with incursions of subtropical species such as *Orbulina universa* at ~136 ka (Fig. 12). Mojtahid *et al.* (2005) also interpreted a warming trend at MD03-2692 from ~151 to ~135 ka. These authors suggested that climatic warming in the tropics related to a shift in the planet's eccentricity significantly warmed the North Atlantic ~151 ka. Following this warm phase, cooling from ~135 to ~129 ka pushed the polar front

Table 6. List of peak IRD horizons at DSDP 548 with high %NPS associated with MIS terminations.

Age (ka)	%NPS	IRD concentration (grains g^{-1})	Event	BIIS phase	Notes
14.6	70	1215	Termination 1	Devensian	End of Devensian BIIS
132	39	1416	Termination 2	Wolstonian	End of Wolstonian BIIS
221	89	2049	Termination 3A		End of MIS 7d BIIS
252	73	1121	Termination 3		End of MIS 8 BIIS

15023885, 0, Downloaded from https://onlinelibrary.wiley.com/doi/10.1111/bor.12631 by National Health And Medical Research Council, Wiley Online Library on [10/08/2023]. See the Terms and Conditions (https://onlinelibrary.wiley.com/terms-and-conditions) on Wiley Online Library for rules of use; OA articles are governed by the applicable Creative Commons License

south of DSDP Site 548 and MD03-2692 in the Bay of Biscay (Mojtahid *et al.* 2005).

A significant IRD peak at ~132 ka, equivalent to HE 11 (Govin *et al.* 2015; Mokeddem & McManus 2016), preceded the glacial conditions of ~129 ka at Site 548. At IODP Site U1308, sediments dated at ~132 ka have high Si/Sr yet low in Ca/Sr ratios (Hodell *et al.* 2008; Fig. 13), suggesting increased 'non-LIS' IRD discharge. The ~132 ka IRD peak is interpreted as a sign of the final massive iceberg discharge event from the Wolstonian BIIS before its retreat during interglacial MIS 5e, followed by a significant reduction or even temporary cessation of IRD deposition from the BIIS.

Marine Isotope Stage 5e (Ipswichian Interglacial). – Following the demise of the Wolstonian BIIS by the end of MIS 6, the climate warmed rapidly and reached its optimum by ~123 ka during MIS 5e. Shackleton *et al.* (2003) documented a marked increase in Euro-Siberian and Mediterranean vegetation and a sharp decline in steppe vegetation in the pollen record at MD95-2042 (Fig. 1; Tagus Abyssal Plain, west offshore of southern Portugal) during this time, suggesting a warming climate. MIS 5e warming began at ~126 ka and culminated by ~123 ka, associated with %NPS and IRD minima at Site 548 in the absence of a BIIS (Fig. 13).

Marine Isotope Stage 5d-2 (Devensian BIIS). – Significant IRD deposition to the Goban Spur from the Devensian BIIS resumed at MIS 5d. Marked fluctuations in %NPS (from 90 to 7%) and IRD concentration (Fig. 13) characterize the instability of the Devensian BIIS initial growth phase. After a minimum during MIS 5e, %NPS and IRD increased until ~111 ka. However, the %NPS was below the polar front threshold of 80%, which, based on the %NPS temperature estimations of Peck *et al.* (2008) and Govin *et al.* (2012), was equivalent to an average SST of ~9 °C. In addition, the presence of transitional and subtropical planktonic foraminifers also suggests that the polar front was north of Site 548 (Fig. 12). Thus, the elevated IRD concentration at ~111 ka in the Goban Spur likely originates from other northwestern European ice sheets north of the BIIS. One possible source for the IRD may be the disintegration of the Fennoscandian Ice Sheet (Fig. 1), which covered most of Norway and the highlands of Sweden during the Herning stadial at ~110 ka (Mangerud *et al.* 2011; Wohlfarth 2013). Subsequently, %NPS minima and the influx of transitional and subtropical planktonic foraminifera suggest more temperate conditions at ~109 ka (Fig. 12). Cooling followed, and by ~99 ka, the polar front was at or south of DSDP Site 548.

The polar front was south of DSDP Site 548 at ~85 and ~60 ka. A significant IRD influx characterized the ~60 ka polar front migration, equivalent to HE 6 (Heinrich 1988), one of the 'non-LIS' types of Heinrich Events (Grousset *et al.* 2000). At MD03-2692 (Bay of Biscay), HE 6 is characterized by high %NPS, increased magnetic intensity values and high IRD concentration with reduced foraminiferal productivity, while at IODP Site U1308, it is characterized by increased detrital carbonate, a magnetic intensity maximum, high Si/Sr and low Ca/Sr ratios (Fig. 13), indicating increased IRD input from the northwestern European ice sheets (Hodell *et al.* 2008).

Throughout MIS 3, %NPS never exceeded 80% at Site 548, indicating sub-polar SST just south of the polar front with the warmest period at ~46 ka. IRD deposition was continuous throughout MIS 3; however, it was not abundant as in either MIS 2 or 4, suggesting a persistent smaller BIIS. The minor IRD peak at ~33 ka may be equivalent to HE 3. However, the %NPS suggests that the polar front was north of Site 548, and the IRD concentration of this event (~400 lithic grains g^{-1}) is lower than the older HE 6 equivalent horizons (~1800 lithic grains g^{-1}) (Fig. 10). This difference suggests that the BIIS was a more prominent IRD contributor to the Atlantic during HE 6, while other northwest European ice sheets north of the BIIS (Fig. 1) may have been the primary HE 3 IRD source. This finding supports the suggestion that there were different IRD sources for HE 3 and HE 6 (Andrews 2000; Hemming 2004). Grousset *et al.* (1993) and Gwiazda *et al.* (1996) suggested that the Fennoscandian and Greenland ice sheets were the primary IRD sources during HE 3.

SST cooled after ~18 ka during MIS 2, with the migration of the polar front to or south of DSDP Site 548 by ~15.6 ka, equivalent to HE 1, associated with increased IRD concentration at Site 548 and MD03-2692 (Mojtahid *et al.* 2005), and increased (minor) HE-type lithics at Site 548. Similar IRD concentration maxima with a LIS signature are also reported at MD01-2461 (Peck *et al.* 2007) and OMEX-2K (Haapaniemi *et al.* 2010), suggesting synchronous iceberg calving from the BIIS and LIS during HE 1.

The increased IRD at ~14.6 ka was associated with sub-polar (70%) %NPS (Fig. 13). This youngest peak IRD horizon may represent the last major iceberg calving from a BIIS that had already detached into discrete ice caps centred in the highlands of Ireland and Scotland by ~15 ka (Clark *et al.* 2022) during the warming period following HE 1 (McCabe *et al.* 1998; Scourse *et al.* 2009). A similar trend is also interpreted from the laminated facies at MD03-2692 from ~16 ka to Termination 1, which, according to Mojtahid *et al.* (2005), represents enhanced seasonal melting of the BIIS during the period. Three IRD horizons at Site 548 may be associated with episodes of BIIS calving at ~60, ~15.6 and ~14.6 ka; associated with HE 6, 1 and the terminal iceberg calving activity from the already detached British and Irish ice sheets (Clark *et al.* 2022).

15023885, 0, Downloaded from https://onlinelibrary.wiley.com/doi/10.1111/bor.12631 by National Health And Medical Research Council, Wiley Online Library on [10/08/2023]. See the Terms and Conditions (https://onlinelibrary.wiley.com/terms-and-conditions) on Wiley Online Library for rules of use; OA articles are governed by the applicable Creative Commons License

Marine Isotope Stage 1 (Holocene). – Dominant subpolar taxa characterize the MIS 1 record at Site 548, with minor %NPS and an influx of subtropical and transitional planktonic foraminiferal assemblages (Fig. 12), associated with minor IRD input at ~12 ka (Fig. 13). The record suggests that the Devensian BIIS's final demise occurred during a Holocene warming background, accompanied by AMOC strengthening and more vigorous ENACW, MOW and NAC, which led to the present day climatic and oceanographic configuration (Figs 4A, 5A).

Conclusions

Using the presented age framework, we combined facies, planktonic foraminiferal assemblage and coarse lithic grain analyses to determine the 250 000-year history of the BIIS and North Atlantic polar front history for the Goban Spur and reached the following conclusions:

- The alternation between pelagic mud and calcium carbonate-rich silty sand contouritic facies (Stow & Faugères 2008) within the top 40 m at Site 548 directly reflects the glacial–interglacial cycle for the past 250 000 years.
- %NPS record of Site 548 indicates multiple North Atlantic polar front migrations south of the Goban Spur during glacial maxima and stadial periods, while the invigoration of the northward flowing MOW during interglacial periods generated contouritic sediments. Our interpretation of a stronger MOW during interglacial periods of the Late Pleistocene agrees with the findings of Kaboth *et al.* (2017).
- Coarse lithic clasts census at Site 548, Ca/Sr and Si/Sr ratios from U1308 (Hodell *et al.* 2008) and IRD concentration at MD03-2692 (Mojtahid *et al.* 2005) reveal that the coarse lithic grains embedded in DSDP Core 548 are IRD from northwest European ice-sheet discharges, principally from the BIIS.
- The peak IRD-rich horizons of Site 548 are grouped based on the %NPS value and their association with glacial MIS termination events. Those associated with the MIS termination events precede a significant reduction in IRD deposition to Site 548, suggesting episodes of major ice shelf collapse preceding a significant retreat of the BIIS. In comparison, those not associated with termination events reflect iceberg calving and IRD deposition related to possible ice shelf formation around the BIIS during the colder period.
- The signatures of the two non-LIS' Heinrich Events (HE), HE 6 and 3, are very different in Site 548. HE 6 (~60 ka) has a polar level of %NPS and IRD concentration more than four times that of HE 3 (~33 ka), and %NPS during HE 3 is below the polar level. Thus, BIIS discharge is a major IRD contributor to the Goban Spur during HE 6, while during HE 3, other northwestern European ice sheets north of the BIIS are more dominant.
- Six distinct IRD peaks are associated with the middle to late Wolstonian BIIS, three of which correspond to the extreme glacial conditions at ~267, ~255 and ~155 ka relating to the migration of the polar front south of Site 548. In contrast, the other three at ~252, ~221 and ~132 ka correspond to Termination 3, 3A and 2, respectively. The IRD peak at ~223 ka (MIS 7d) signifies increased BIIS activity during the extremely cold yet short-lived stadial period (Hughes *et al.* 2020), while the IRD peak at ~132 ka signifies the last major iceberg calving from the Wolstonian BIIS.
- Significant IRD deposition from the Devensian BIIS resumes from MIS 5d, with three significant peaks at 60, 15.5 and 14.6 ka. The two oldest peaks are coeval to HE 6 and 1, whilst the youngest peak reflects one of the last significant icebergs calving from the Devensian BIIS before its demise.

Acknowledgements. – An Australian Government Research Training Program Scholarship supports Stanislaus G. Fabian. Funding was provided to SJG by the Australian IODP office. The authors thank IODP Bremen Core Repository for granting access to inspect and sample DSDP Core 548. Thanks are due to Artur Fugmann for laboratory assistance and support on the mass spectrometers at the University of Münster. A special thanks to Frédérique Eynaud and Samuel Toucanne, who kindly provided the MD03-2692 data sets and generously reviewed and provided valuable suggestions for the early draft of this paper. The authors are indebted to Jan A. Piotrowski for the editorial support, and Karen Luise Knudsen and anonymous referees for manuscript review. Open access publishing facilitated by The University of Melbourne, as part of the Wiley - The University of Melbourne agreement via the Council of Australian University Librarians.

Author contributions. – SJG and SGF conceived the study. SGF led the data acquisition, sample collection, preparation, and analyses, along with data synthesis and writing of the manuscript with guidance from SJG and DDV. DDV wrote the 'Benthic foraminifera stable isotope analysis' in the Material and methods section and provided stable isotope measurements from samples prepared by SGF. SGF revised the final manuscript incorporating inputs from SJG, DDV, the managing editor and other reviewers.

Data availability statement. – All data associated with this study are available from the corresponding author upon reasonable request.

References

Andrews, J. T. 2000: Icebergs and iceberg rafted detritus (IRD) in the North Atlantic: facts and assumptions. *Oceanography 13*, 100–108.

Andrews, J. T. & Voelker, A. H. 2018: "Heinrich events" (& sediments): a history of terminology and recommendations for future usage. *Quaternary Science Reviews 187*, 31–40.

Barker, S., Chen, J., Gong, X., Jonkers, L., Knorr, G. & Thornalley, D. 2015: Icebergs not the trigger for North Atlantic cold events. *Nature 520*, 333–336.

Barker, S., Knorr, G., Conn, S., Lordsmith, S., Newman, D. & Thornalley, D. J. R. 2019: Foraminifer and IRD counts from ODP Site 162-983. Supplement to: Barker, S. *et al.* (2019): Early interglacial

15023885, 0, Downloaded from https://onlinelibrary.wiley.com/doi/10.1111/bor.12631 by National Health And Medical Research Council, Wiley Online Library on [10/08/2023]. See the Terms and Conditions (https://onlinelibrary.wiley.com/terms-and-conditions) on Wiley Online Library for rules of use; OA articles are governed by the applicable Creative Commons License

legacy of deglacial climate instability. *Paleoceanography and Paleoclimatology 34*, 1455–1475.
Bashirova, L. D., Kandiano, E. S., Sivkov, V. V. & Bauch, H. A. 2014: Migrations of the North Atlantic Polar front during the last 300 ka: evidence from planktic foraminiferal data. *Oceanology 54*, 798–807.
Batchelor, C. L., Margold, M., Krapp, M., Murton, D. K., Dalton, A. S., Gibbard, P. L., Stokes, C. R., Murton, J. B. & Manica, A. 2019: The configuration of Northern Hemisphere ice sheets through the Quaternary. *Nature Communications 10*, 3713, https://doi.org/10.1038/41467-019-11601-2.
Bond, G. C. & Lotti, R. 1995: Iceberg discharges into the North Atlantic on millennial time scales during the last glaciation. *Science 267*, 1005–1010.
Bond, G., Heinrich, H., Broecker, W., Labeyrie, L., McManus, J., Andrews, J., Huon, S., Jantschik, R., Clasen, S. & Simet, C. 1992: Evidence for massive discharges of icebergs into the North Atlantic ocean during the last glacial period. *Nature 360*, 245–249.
Bradley, S. L., Ely, J. C., Clark, C. D., Edwards, R. J. & Shennan, I. 2023: Reconstruction of the palaeo-sea level of Britain and Ireland arising from empirical constraints of ice extent: implications for regional sea level forecasts and North American ice sheet volume. *Journal of Quaternary Science*, Advance online publication, https://doi.org/10.1002/jqs.3523.
Bradwell, T., Small, D., Fabel, D., Clark, C. D., Chiverrell, R. C., Saher, M. H., Dove, D., Callard, S. L., Burke, M. J. & Moreton, S. G. 2021: Pattern, style and timing of British–Irish Ice Sheet retreat: Shetland and northern North Sea sector. *Journal of Quaternary Science 36*, 681–722.
Chennaux, G., Esquevin, J., Jourdan, A., Latouche, C. & Maillet, N. 1985: X-Ray mineralogy and mineral geochemistry of Cenozoic strata (Leg-80) and petrographic study of associated pebbles. *Initial Reports of the Deep Sea Drilling Project 80*, 1019–1046.
Clark, C. D., Ely, J. C., Hindmarsh, R. C., Bradley, S., Ignéczi, A., Fabel, D., Ó Cofaigh, C., Chiverrell, R. C., Scourse, J. & Benetti, S. 2022: Growth and retreat of the last British–Irish Ice Sheet, 31 000 to 15 000 years ago: the BRITICE-CHRONO reconstruction. *Boreas 51*, 699–758.
Clark, C. D., Hughes, A. L., Greenwood, S. L., Jordan, C. & Sejrup, H. P. 2012: Pattern and timing of retreat of the last British-Irish Ice Sheet. *Quaternary Science Reviews 44*, 112–146.
Colin, J. P., Ioannides, N. S. & Vining, B. 1992: Mesozoic stratigraphy of the Goban Spur, offshore south-west Ireland. *Marine and Petroleum Geology 9*, 527–541.
Couette, P. O., Lajeunesse, P., Ghienne, J. F., Dorschel, B., Gebhardt, C., Hebbeln, D. & Brouard, E. 2022: Evidence for an extensive ice shelf in northern Baffin Bay during the Last Glacial Maximum. *Communications Earth & Environment 3*, 225, https://doi.org/10.1038/s43247-022-00559-7.
Dalton, A. S. and 70 others. 2020: An updated radiocarbon-based ice margin chronology for the last deglaciation of the North American Ice Sheet Complex. *Quaternary Science Reviews 234*, 106223, https://doi.org/10.1016/j.quascirev.2020.106223.
De Graciansky, P. C., Poag, C., Cunningham, R., Loubere, P., Masson, D., Mazzullo, J., Montadert, L., Müller, C., Otsuka, K. & Reynolds, L. 1985: Site 548. *Initial Reports of the Deep Sea Drilling Project 80*, 33–122.
Delaney, C. 2003: The last glacial stage (the Devensian) in Northwest England. *North West Geography 3*, 27–37.
Delivet, S., Van Eetvelt, B., Monteys, X., Ribó, M. & Van Rooij, D. 2016: Seismic geomorphological reconstructions of Plio-Pleistocene bottom current variability at Goban Spur. *Marine Geology 378*, 261–275.
Eynaud, F., de Abreu, L., Voelker, A., Schönfeld, J., Salgueiro, E., Turon, J. L., Penaud, A., Toucanne, S., Naughton, F., Sánchez Goñi, M. F., Malaizé, B. & Cacho, I. 2009: Position of the Polar Front along the western Iberian margin during key cold episodes of the last 45 ka. *Geochemistry, Geophysics, Geosystems 10*, Q07U05, https://doi.org/10.1029/2009GC002398.
Eynaud, F., Zaragosi, S., Scourse, J., Mojtahid, M., Bourillet, J. F., Hall, I. R., Penaud, A., Locascio, M. & Reijonen, A. 2007: Deglacial laminated facies on the NW European continental margin: the hydrographic significance of British-Irish Ice Sheet deglaciation and Fleuve Manche paleoriver discharges. *Geochemistry, Geophysics, Geosystems 8*, Q06019, https://doi.org/10.1029/2006GC001496.
Gibbard, P. & Cohen, K. M. 2008: Global chronostratigraphical correlation table for the last 2.7 million years. *Episodes 31*, 243–247.
Gibbard, P. L., Hughes, P. D., Clark, C. D., Glasser, N. F. & Tomkins, M. D. 2022: Chapter 34 – Britain and Ireland: glacial landforms prior to the Last Glacial Maximum. *In* Palacios, D., Hughes, P. D., García-Ruiz, J. M. & Andrés, N. (eds.): *European Glacial Landscapes*, 245–253. Elsevier, Amsterdam.
Gibbard, P. L., Pasanen, A. H., West, R. G., Lunkka, J. P., Boreham, S., Cohen, K. M. & Rolfe, C. 2009: Late middle Pleistocene glaciation in east Anglia, England. *Boreas 38*, 504–528.
Govin, A., Braconnot, P., Capron, E., Cortijo, E., Duplessy, J. C., Jansen, E., Labeyrie, L., Landais, A., Marti, O., Michel, E., Mosquet, E., Risebrobakken, B., Swingedouw, D. & Waelbroeck, C. 2012: Persistent influence of ice sheet melting on high northern latitude climate during the early Last Interglacial. *Climate of the Past 8*, 483–507.
Govin, A., Capron, E., Tzedakis, P. C., Verheyden, S., Ghaleb, B., Hillaire-Marcel, C., St-Onge, G., Stoner, J. S., Bassinot, F., Bazin, L., Blunier, T., Combourieu-Nebout, N., El Ouahabi, A., Genty, D., Gersonde, R., Jimenez-Amat, P., Landais, A., Martrat, B., Masson-Delmotte, V., Parrenin, F., Seidenkrantz, M. S., Veres, D., Waelbroeck, C. & Zahn, R. 2015: Sequence of events from the onset to the demise of the Last Interglacial: evaluating strengths and limitations of chronologies used in climatic archives. *Quaternary Science Reviews 129*, 1–36.
Grootes, P. M., Stuiver, M., White, J., Johnsen, S. & Jouzel, J. 1993: Comparison of oxygen isotope records from the GISP2 and GRIP Greenland ice cores. *Nature 366*, 552–554.
Grousset, F., Labeyrie, L., Sinko, J., Cremer, M., Bond, G., Duprat, J., Cortijo, E. & Huon, S. 1993: Patterns of ice-rafted detritus in the glacial North Atlantic (40–55° N). *Paleoceanography 8*, 175–192.
Grousset, F. E., Pujol, C., Labeyrie, L., Auffret, G. & Boelaert, A. 2000: Were the North Atlantic Heinrich events triggered by the behavior of the European ice sheets? *Geology 28*, 123–126.
Gwiazda, R. H., Hemming, S. R. & Broecker, W. S. 1996: Provenance of icebergs during Heinrich Event 3 and the contrast to their sources during other Heinrich episodes. *Paleoceanography 11*, 371–378.
Haapaniemi, A. I., Scourse, J. D., Peck, V. L., Kennedy, H., Kennedy, P., Hemming, S. R., Furze, M. F., Pieńkowski, A. J., Austin, W. E. N., Walden, J., Wadsworth, E. & Hall, I. R. 2010: Source, timing, frequency and flux of ice-rafted detritus to the northeast Atlantic margin, 30–12 ka: testing the Heinrich precursor hypothesis. *Boreas 39*, 576–591.
Hamblin, R., Moorlock, B., Rose, J., Lee, J., Riding, J., Booth, S. & Pawley, S. 2005: Revised Pre-Devensian glacial stratigraphy in Norfolk, England, based on mapping and till provenance. *Netherlands Journal of Geosciences 84*, 77–85.
Heinrich, H. 1988: Origin and consequences of cyclic ice rafting in the northeast Atlantic Ocean during the past 130,000 years. *Quaternary Research 29*, 142–152.
Hemming, S. R. 2004: Heinrich events: massive late Pleistocene detritus layers of the North Atlantic and their global climate imprint. *Reviews of Geophysics 42*, 1–43.
Hemming, S., Broecker, W., Sharp, W., Bond, G., Gwiazda, R., McManus, J., Klas, M. & Hajdas, I. 1998: Provenance of Heinrich layers in core V28-82, northeastern Atlantic: $^{40}Ar/^{39}Ar$ ages of ice-rafted hornblende, Pb isotopes in feldspar grains, and Nd–Sr–Pb isotopes in the fine sediment fraction. *Earth and Planetary Science Letters 164*, 317–333.
Hodell, D. A., Channell, J. E., Curtis, J. H., Romero, O. E. & Röhl, U. 2008: Onset of "Hudson Strait" Heinrich events in the eastern North Atlantic at the end of the middle Pleistocene transition (~ 640 ka)? *Paleoceanography 23*, PA4218, https://doi.org/10.1029/2008PA001591.
Holliday, N. P., Hughes, S., Bacon, S., Beszczynska-Möller, A., Hansen, B., Lavin, A., Loeng, H., Mork, K., Østerhus, S. & Sherwin, T. 2008: Reversal of the 1960s to 1990s freshening trend in the Northeast North Atlantic and Nordic Seas. *Geophysical Research Letters 35*, L03614, https://doi.org/10.1029/2007GL032675.

15023885, 0, Downloaded from https://onlinelibrary.wiley.com/doi/10.1111/bor.12631 by National Health And Medical Research Council, Wiley Online Library on [10/08/2023]. See the Terms and Conditions (https://onlinelibrary.wiley.com/terms-and-conditions) on Wiley Online Library for rules of use; OA articles are governed by the applicable Creative Commons License

Hughes, P. D., Gibbard, P. L. & Ehlers, J. 2020: The "missing glaciations" of the Middle Pleistocene. *Quaternary Research 96*, 161–183.
Hughes, P. D., Palacios, D., García-Ruiz, J. M. & Andrés, N. 2022: Chapter 45 – The European glacial landscapes prior to the Last Glacial Maximum – synthesis. *In* Palacios, D., Hughes, P. D., García-Ruiz, J. M. & Andrés, N. (eds.): *European Glacial Landscapes*, 341–351. Elsevier, Amsterdam.
Jost, L. 2006: Entropy and diversity. *Oikos 113*, 363–375.
Huelsemann, J. 1966: On the routine analysis of carbonates in unconsolidated sediments. *Journal of Sedimentary Research 36*, 622–625.
Kaboth, S., de Boer, B., Bahr, A., Zeeden, C. & Lourens, L. J. 2017: Mediterranean outflow water dynamics during the past ~570 kyr: regional and global implications. *Paleoceanography 32*, 634–647.
Kenyon, N., Belderson, R. & Stride, A. 1978: Channels, canyons and slump folds on continental slope between southwest Ireland and Spain. *Oceanologica Acta 1*, 369–380.
Knutz, P. C., Austin, W. E. & Jones, E. J. W. 2001: Millennial-scale depositional cycles related to British Ice Sheet variability and North Atlantic paleocirculation since 45 kyr BP, Barra Fan, UK margin. *Paleoceanography 16*, 53–64.
Knutz, P. C., Zahn, R. & Hall, I. R. 2007: Centennial-scale variability of the British Ice Sheet: implications for climate forcing and Atlantic meridional overturning circulation during the last deglaciation. *Paleoceanography 22*, PA1207, https://doi.org/10.1029/2006PA001298.
van Kreveld, S. 1996: Northeast Atlantic late Quaternary planktic foraminifera as primary productivity and water mass indicators. *Scripta Geologica 113*, 23–91.
van Kreveld, S., Sarnthein, M., Erlenkeuser, H., Grootes, P., Jung, S., Nadeau, M., Pflaumann, U. & Voelker, A. 2000: Potential links between surging ice sheets, circulation changes, and the Dansgaard-Oeschger cycles in the Irminger Sea, 60–18 kyr. *Paleoceanography 15*, 425–442.
Kucera, M. 2007: Chapter 6 – Planktonic foraminifera as tracers of past oceanic environments. *In* Hillaire-Marcel, C. & de Vernal, A. (eds.): *Proxies in Late Cenozoic Paleoceanography*, 213–262. Elsevier, Amsterdam.
Lacasse, C., Sigurdsson, H., Carey, S., Paterne, M. & Guichard, F. 1996: North Atlantic deep-sea sedimentation of Late Quaternary tephra from the Iceland hotspot. *Marine Geology 129*, 207–235.
Lee, J. R., Rose, J., Hamblin, R. J. O., Moorlock, B. S. P., Riding, J. B., Phillips, E., Barendregt, R. W. & Candy, I. 2011: Chapter 6 – The glacial history of the British Isles during the Early and Middle Pleistocene: implications for the long-term development of the British Ice Sheet. *In* Ehlers, J., Gibbard, P. L. & Hughes, P. D. (eds.): *Developments in Quaternary Sciences*, 59–74. Elsevier, Amsterdam.
Lisiecki, L. E. & Raymo, M. E. 2005: A Pliocene-Pleistocene stack of 57 globally distributed benthic $\delta^{18}O$ records. *Paleoceanography 20*, PA1003, https://doi.org/10.1029/2004PA001071.
Loubere, P. 1987: Changes in mid-depth North Atlantic and Mediterranean circulation during the Late Pliocene—Isotopic and sedimentological evidence. *Marine Geology 77*, 15–38.
Mangerud, J., Gyllencreutz, R., Lohne, Ä. & Svendsen, J. I. 2011: Chapter 22 – Glacial history of Norway. *In* Ehlers, J., Gibbard, P. L. & Hughes, P. D. (eds.): *Developments in Quaternary Sciences*, 279–298. Elsevier, Amsterdam.
Marchal, O., Waelbroeck, C. & Colin de Verdière, A. 2016: On the movements of the North Atlantic subpolar front in the preinstrumental past. *Journal of Climate 29*, 1545–1571.
McCabe, M., Knight, J. & McCarron, S. 1998: Evidence for Heinrich event 1 in the British Isles. *Journal of Quaternary Science 13*, 549–568.
Mojtahid, M., Eynaud, F., Zaragosi, S., Scourse, J., Bourillet, J. F. & Garlan, T. 2005: Palaeoclimatology and palaeohydrography of the glacial stages on Celtic and Armorican margins over the last 360000 yrs. *Marine Geology 224*, 57–82.
Mokeddem, Z. & McManus, J. F. 2016: Persistent climatic and oceanographic oscillations in the subpolar North Atlantic during the MIS 6 glaciation and MIS 5 interglacial. *Paleoceanography 31*, 758–778.
Moreau, J., Huuse, M., Janszen, A., van der Vegt, P., Gibbard, P. L. & Moscariello, A. 2012: The glaciogenic unconformity of the southern North Sea. *Geological Society, London, Special Publications 368*, 99–110.
Nørgaard-Pedersen, N., Mikkelsen, N. & Kristoffersen, Y. 2007: Arctic Ocean record of last two glacial-interglacial cycles off North Greenland/Ellesmere Island—implications for glacial history. *Marine Geology 244*, 93–108.
Olsen, L., Sveian, H., Bergstrøm, B., Ottesen, D. & Rise, L. 2013: Quaternary glaciations and their variations in Norway and on the Norwegian continental shelf. *Quaternary Geology of Norway 13*, 27–78.
Ovsepyan, E. A. & Murdmaa, I. O. 2017: Response of the bering sea to Heinrich Event 11. *Lithology and Mineral Resources 52*, 442–446.
Peck, V. L. 2017: Paleoclimate records from core MD01-2461, Porcupine Seabight, NE Atlantic. *PANGAEA*. https://doi.org/10.1594/PANGAEA.221722.
Peck, V. L., Hall, I. R., Zahn, R. & Elderfield, H. 2008: Millennial-scale surface and subsurface paleothermometry from the Northeast Atlantic, 55–8 ka BP. *Paleoceanography 23*, PA3221, https://doi.org/10.1029/2008PA001631.
Peck, V. L., Hall, I. R., Zahn, R., Elderfield, H., Grousset, F., Hemming, S. R. & Scourse, J. D. 2006: High resolution evidence for linkages between NW European ice sheet instability and Atlantic Meridional Overturning Circulation. *Earth and Planetary Science Letters 243*, 476–488.
Peck, V. L., Hall, I. R., Zahn, R., Grousset, F., Hemming, S. & Scourse, J. 2007: The relationship of Heinrich events and their European precursors over the past 60 ka BP: a multi-proxy ice-rafted debris provenance study in the North East Atlantic. *Quaternary Science Reviews 26*, 862–875.
Penaud, A., Eynaud, F., Turon, J., Zaragosi, S., Marret, F. & Bourillet, J.-F. 2008: Interglacial variability (MIS 5 and MIS 7) and dinoflagellate cyst assemblages in the Bay of Biscay (North Atlantic). *Marine Micropaleontology 68*, 136–155.
Peters, J. L., Benetti, S., Dunlop, P. & Ó Cofaigh, C. 2015: Maximum extent and dynamic behaviour of the last British–Irish Ice Sheet west of Ireland. *Quaternary Science Reviews 128*, 48–68.
Peters, J. L., Benetti, S., Dunlop, P., Ó Cofaigh, C., Moreton, S. G., Wheeler, A. J. & Clark, C. D. 2016: Sedimentology and chronology of the advance and retreat of the last British-Irish Ice Sheet on the continental shelf west of Ireland. *Quaternary Science Reviews 140*, 101–124.
Pingree, R. D. & Le Cann, B. 1990: Structure, strength and seasonality of the slope currents in the Bay of Biscay region. *Journal of the Marine Biological Association of the United Kingdom 70*, 857–885.
Railsback, L. B., Gibbard, P. L., Head, M. J., Voarintsoa, N. R. G. & Toucanne, S. 2015: An optimized scheme of lettered marine isotope substages for the last 1.0 million years, and the climatostratigraphic nature of isotope stages and substages. *Quaternary Science Reviews 111*, 94–106.
Ravelo, A. C. & Hillaire-Marcel, C. 2007: Chapter 18 – The use of oxygen and carbon isotopes of foraminifera in paleoceanography. *In* Hillaire–Marcel, C. & De Vernal, A. (eds.): *Developments in Marine Geology*, 735–764. Elsevier, Amsterdam.
Roucoux, K., Tzedakis, P., De Abreu, L. & Shackleton, N. 2006: Climate and vegetation changes 180,000 to 345,000 years ago recorded in a deep-sea core off Portugal. *Earth and Planetary Science Letters 249*, 307–325.
Ruddiman, W. F., Raymo, M. E., Martinson, D. G., Clement, B. M. & Backman, J. 1989: Pleistocene evolution: Northern hemisphere ice sheets and North Atlantic Ocean. *Paleoceanography 4*, 353–412.
Schlitzer, R. 2023: Ocean data view. Available at: https://odv.awi.de.
Scourse, J. D., Chiverrell, R. C., Smedley, R. K., Small, D., Burke, M. J., Saher, M., Van Landeghem, K. J. J., Duller, G. A. T., Ó Cofaigh, C., Bateman, M. D., Benetti, S., Bradley, S., Callard, L., Evans, D. J. A., Fabel, D., Jenkins, G. T. H., McCarron, S., Medialdea, A., Moreton, S., Ou, X., Praeg, D., Roberts, D. H., Roberts, H. M. & Clark, C. D. 2021: Maximum extent and readvance dynamics of the Irish Sea Ice Stream and Irish Sea Glacier since the Last Glacial Maximum. *Journal of Quaternary Science 36*, 780–804.
Scourse, J. D., Haapaniemi, A. I., Colmenero-Hidalgo, E., Peck, V. L., Hall, I. R., Austin, W. E. N., Knutz, P. C. & Zahn, R. 2009: Growth, dynamics and deglaciation of the last British–Irish Ice Sheet: the

15023885, 0, Downloaded from https://onlinelibrary.wiley.com/doi/10.1111/bor.12631 by National Health And Medical Research Council, Wiley Online Library on [10/08/2023]. See the Terms and Conditions (https://onlinelibrary.wiley.com/terms-and-conditions) on Wiley Online Library for rules of use; OA articles are governed by the applicable Creative Commons License

deep-sea ice-rafted detritus record. *Quaternary Science Reviews 28*, 3066–3084.
Scourse, J. D., Hall, I. R., McCave, I. N., Young, J. R. & Sugdon, C. 2000: The origin of Heinrich layers: evidence from H2 for European precursor events. *Earth and Planetary Science Letters 182*, 187–195.
Scourse, J., Ward, S., Wainwright, A., Bradley, S. & Uehara, K. 2018: The role of megatides and relative sea level in controlling the deglaciation of the British–Irish and Fennoscandian ice sheets. *Journal of Quaternary Science 33*, 139–149.
Shackleton, N. J., Sánchez-Goñi, M. F., Pailler, D. & Lancelot, Y. 2003: Marine isotope substage 5e and the Eemian interglacial. *Global and Planetary Change 36*, 151–155.
Shannon, C. E. 1948: A mathematical theory of communication. *The Bell System Technical Journal 27*, 379–423.
Shotton, F. W. 1983: The Wolstonian stage of the british pleistocene in and around its type area of the english midlands. *Quaternary Science Reviews 2*, 261–280.
Snyder, S. & Waters, V. 1985: Cenozoic planktonic foraminiferal biostratigraphy of the Goban Spur region, Deep Sea Drilling Project Leg 80. *Initial Reports of the Deep Sea Drilling Project 80*, 439–472.
Spellerberg, I. F. & Fedor, P. J. 2003: A tribute to Claude Shannon (1916–2001) and a plea for more rigorous use of species richness, species diversity and the 'Shannon–Wiener' Index. *Global Ecology and Biogeography 12*, 177–179.
Stein, R., Hefter, J., Grützner, J., Voelker, A. & Naafs, B. D. A. 2009: Variability of surface water characteristics and Heinrich-like events in the Pleistocene midlatitude North Atlantic Ocean: biomarker and XRD records from IODP Site U1313 (MIS 16–9). *Paleoceanography 24*, PA2203, https://doi.org/10.1029/2008PA001639.
Stow, D. & Faugères, J. C. 2008: Contourite facies and the facies model. *Developments in Sedimentology 60*, 223–256.
Thierens, M., Pirlet, H., Colin, C., Latruwe, K., Vanhaecke, F., Lee, J. R., Stuut, J. B., Titschack, J., Huvenne, V. A. I., Dorschel, B., Wheeler, A. J. & Henriet, J. P. 2012: Ice-rafting from the British–Irish Ice Sheet since the earliest Pleistocene (2.6 million years ago): implications for long-term mid-latitudinal ice-sheet growth in the North Atlantic region. *Quaternary Science Reviews 44*, 229–240.
Toucanne, S., Zaragosi, S., Bourillet, J. F., Cremer, M., Eynaud, F., Van Vliet-Lanoë, B., Pénaud, A., Fontanier, C., Turon, J. & Cortijo, E. 2009: Timing of massive 'Fleuve Manche' discharges over the last 350 kyr: insights into the European ice-sheet oscillations and the European drainage network from MIS 10 to 2. *Quaternary Science Reviews 28*, 1238–1256.
Tzedakis, P., McManus, J., Hooghiemstra, H., Oppo, D. & Wijmstra, T. 2003: Comparison of changes in vegetation in Northeast Greece with records of climate variability on orbital and suborbital frequencies over the last 450 000 years. *Earth and Planetary Science Letters 212*, 197–212.
Van Aken, H. M. 2000: The hydrography of the mid-latitude Northeast Atlantic Ocean. *Deep Sea Research Part I: Oceanographic Research Papers 47*, 789–824.
Van Rooij, D., Blamart, D., Richter, T., Wheeler, A., Kozachenko, M. & Henriet, J. P. 2006: Quaternary sediment dynamics in the Belgica mound province, Porcupine Seabight: ice-rafting events and contour current processes. *International Journal of Earth Sciences 96*, 121–140.
Van Rooij, D., Iglesias, J., Hernández-Molina, F. J., Ercilla, G., Gomez-Ballesteros, M., Casas, D., Llave, E., De Hauwere, A., García-Gil, S. & Acosta, J. 2010: The Le Danois Contourite Depositional System: interactions between the Mediterranean outflow water and the upper Cantabrian slope (North Iberian margin). *Marine Geology 274*, 1–20.
Verweirder, L., Van Rooij, D., White, M., Van Landeghem, K., Bossée, K. & Georgiopoulou, A. 2021: Combined control of bottom and turbidity currents on the origin and evolution of channel systems, examples from the Porcupine Seabight. *Marine Geology 442*, 106639, https://doi.org/10.1016/j.margeo.2021.106639.
Vigilante, T., Ondei, S., Goonack, C., Williams, D., Young, P. & Bowman, D. M. J. S. 2017: Collaborative research on the ecology and management of the 'Wulo' monsoon rainforest in Wunambal Gaambera Country, North Kimberley, Australia. *Land 6*, 68, https://doi.org/10.3390/land6040068.
Wallace, M. W., Holdgate, G. R., Daniels, J., Gallagher, S. J. & Smith, A. 2002: Sonic velocity, submarine canyons, and burial diagenesis in oligocene-holocene cool-water carbonates, gippsland basin, southeast Australia. *AAPG Bulletin 86*, 1593–1607.
Weaver, P. P., Wynn, R. B., Kenyon, N. H. & Evans, J. 2000: Continental margin sedimentation, with special reference to the north-east Atlantic margin. *Sedimentology 47*, 239–256.
Williamson, G. J., Boggs, G. S. & Bowman, D. M. J. S. 2011: Late 20th century mangrove encroachment in the coastal Australian monsoon tropics parallels the regional increase in woody biomass. *Regional Environmental Change 11*, 19–27.
Wohlfarth, B. 2013: A review of Early Weichselian climate (MIS 5d-a) in Europe. *Technical report/Svensk kärnbränslehantering AB 44*, 70.

Supporting Information

Additional Supporting Information to this article is available at http://www.boreas.dk.

Data S1. DSDP 548 age model.

Data S2. DSDP 548 planktonic foraminifera counts.

Fig. S1. Tie points for the depth conversion from DSDP 548-A to DSDP 548 for the DSDP 548-A natural gamma radiation (NGR) data (De Graciansky *et al*. 1985). Black dashed lines indicate correlation points. %$CaCO_3$ is used to correct the data as low % $CaCO_3$ and high NGR indicate sediments with high mud content and vice versa. m b.s.f. = metres below sea floor; API = American Petroleum Institute (a unit for natural gamma radiation).

Fig. S2. Scatterplot indicating the relationship between %$CaCO_3$ and %NPS at DSDP Site 548.

Fig. S3. DSDP 548 age bracketing based on pattern correlation of %NPS, %$CaCO_3$, and NGR measurements to the LR04 benthic oxygen isotope curve (Lisiecki & Raymo 2005).

Fig. S4. Additional age tie points based on %NPS correlation between DSDP Site 548 and MD03-2692 (Mojtahid *et al*. 2005; Toucanne *et al*. 2009). m b.s.f. = metres below the sea floor.

Fig. S5. Linear sedimentation rate and age-depth relationship of DSDP Site 548. m b.s.f. = metres below the sea floor.

Fig. S6. Comparison of %NPS from DSDP 548 (this work), ODP 983 (Barker *et al*. 2019), MD01-2461 (Peck 2017) and MD03-2692 (Mojtahid *et al*. 2005; Toucanne *et al*. 2009). Red vertical lines indicate the 7e and 7c interstadials. The blue vertical line indicates the MIS 7d stadial.

15023885, 0, Downloaded from https://onlinelibrary.wiley.com/doi/10.1111/bor.12631 by National Health And Medical Research Council, Wiley Online Library on [10/08/2023]. See the Terms and Conditions (https://onlinelibrary.wiley.com/terms-and-conditions) on Wiley Online Library for rules of use; OA articles are governed by the applicable Creative Commons License